IR 80-2013 (R)

MHD MATERIALS - SEED/SLAG INTERACTIONS AND EFFECTS

QUARTERLY PROGRESS REPORT

October - December 1979

Samuel J. Schneider
Project Manager

Center for Materials Science
National Bureau of Standards
Washington, D. C. 20234

PREPARED FOR THE UNITED STATES
DEPARTMENT OF ENERGY
MHD OFFICE

TABLE OF CONTENTS

I. SUMMARY OF PROGRESS TO DATE

1. Thermochemistry of Seed and Slag

Measurements of the K pressure over the phases orthorhombic $KAlSiO_4$-leucite-beta alumina were begun. The vapor pressure measured with approximately 1/2 the $KAlSiO_4$ phase remaining is about four times higher than the vapor pressure over the K_2O-$9Al_2O_3$-Al_2O_3 two phase mixture.

Equilibrium relations among solid phases in the more K_2O-rich parts of the systems K_2O-Al_2O_3-SiO_2 and K_2O-CaO-Al_2O_3-SiO_2 have been explored. Evidence has been found for the existence of previously unreported compounds of significance in seed/slag reaction.

2. Electrical Conductivity and Polarization

The dependence of the electrical conductivity of $Y_{.95}Ca_{.05}CrO_3$ on oxygen pressure in the range of pressures from 10^0 to 10^{-6} atmospheres have been completed for temperatures from 1300° to 1600° C. The apparatus has been rebuilt to allow measurements in the high temperature range at oxygen pressure from 10^{-6} to 10^{-15} atmospheres.

A three probe electrochemical cell has ben constructed and the electrochemical effects measured at a temperature of 1254° C. This cell allows the measurement of slag-electrode voltages as a function of time and ultimate analyses of the electrochemical effects.

The first series of experiments on the electrical conductivity of Bow NH slag has been completed. The conductivity at low temperatures (below 110° C) depends on the crystalline state of the slag. The conductivity at high temperature (above 1400° C) is independent of the oxygen pressure and of the amount of K present at least up to 6% by weight.

3. Corrosion of Downstream Components

Type 304 stainless tell tubes, cooled to 400° C, 500° C and 590° C, were exposed to fuel rich and oxygen rich hot gas streams seeded with a mixture of 80% by weight K_2CO_3 and 20% by weight K_2SO_4. Optical and SEM and EDX analysis revealed differences, geometrical and chemical, in the deposit formed on the tubing on a result of the tube temperature and the gas stream state. Tubes at the higher temperatures had thinner deposits as did tubes exposed to the fuel rich gas streams. Information with respect to the distribution of Fe, Cr and Ni in the reaction zone (stainless steel-deposit interface) was also obtained with Fe appearing to be the species penetrating most deeply into the salt deposit.

In the coming quarter exposure tests, similar to those conducted on type 304 stainless steel, will be initiated on type 316 stainless steel.

II. DETAILED DESCRIPTION OF TECHNICAL PROGRESS

1. Thermochemistry of Seed and Slag (E. Plante and L. Cook)

A. Vaporization Studies (E. Plante)

Progress: The vaporization section of the thermochemistry of seed and slag task involves the determination of the K_2O activity in simplified slag solutions. These studies will initially be limited to selected subsections of the four component system K_2O-CaO-Al_2O_3-SiO_2 while later studies will include Fe_2O_3 as a component. The overall aim of the vaporization section is to determine the K_2O activity as a function of temperature and selected limited composition ranges. The limits on composition will be generally dictated by the compositions which are likely to be obtained in the combustion of seeded coal.

Determination of the K_2O activity is made by measurement of the $K(g)$ and $O_2(g)$ pressure from slag samples using the Knudsen effusion method coupled with modulated beam mass spectrometric analysis of the vaporization products. The typical vaporization reaction will be,

$$K_2O \text{ (dissolved in slag)} = 2K(g) + 1/2\ O_2(g) \qquad (1)$$

In general, the activity of K_2O with respect to the gaseous phase can be defined as,

$$A_{K_2O} = P_K^2 \cdot P_{O_2}^{\ 1/2} \qquad (2)$$

or with respect to a reference state such as pure liquid K_2O as,

$$A_{K_2O} = \frac{P_K^2 \cdot P_{O_2}^{\ 1/2} \quad \text{over slag}}{P_K^2 \cdot P_{O_2}^{\ 1/2} \quad \text{over pure } K_2O(1)} \qquad (3)$$

The compound, orthorhombic $KAlSiO_4$ is of great importance in the study of seed-slag interaction as it is a major crystalline product in seeded coal slags. The phase diagram as well as previous vaporization studies at NBS indicate that vaporization of K and O_2 from $KAlSiO_4$ should result in formation of leucite ($K_2O \cdot Al_2O_3 \cdot 4SiO_2$) and beta alumina. Beta alumina has a wide composition range which extends from the composition $K_2O \cdot 5Al_2O_3$ to $K_2O \cdot 9Al_2O_3$. Over this composition range the pressure of K varies by a factor of more than 100. Assuming that the beta alumina formed is at the K_2O rich phase boundary (which is not possible for thermodynamic reasons) the reaction for decomposition of $KAlSiO_4$ would be,

$$5KAlSiO_4 = 5/4\ K_2O \cdot Al_2O_3 \cdot 4SiO_2 + 1/4\ K_2O \cdot 5Al_2O_3 + 2K + 1/2\ O_2 \qquad (4)$$

If the beta alumina formed has the composition at the K_2O poor phase boundary, the reaction for decomposition of $KAlSiO_4$ would be,

$$36/8\ KAlSiO_4 = 9/8\ K_2O \cdot Al_2O_3 \cdot 4SiO_2 + 1/8\ K_2O \cdot 9Al_2O_3 + 2K(g) + 1/2\ O_2(g) \quad (5)$$

Reaction 5 has the property that the K pressure should depend only on temperature and be independent of bulk composition since it is a four phase three component system. The vapor pressure curve in this region of the phase diagram will, therefore, serve as a useful reference curve characteristic of a system containing $KAlSiO_4$. Measurements at lower potassia concentrations may be useful because they will be carried out with the system partially in the liquid phase which will be true of many slag systems. Finally, these data will be useful as references for more complex slag solutions containing additional oxides such as CaO or Fe_2O_3.

In previous attempts to measure the K pressure over the $KAlSiO_4$-$K_2O \cdot Al_2O_3 \cdot 4SiO_2$- beta alumina system it was found that a steady state K pressure could not be obtained. This was attributed to the complexity of the crystalline transformation which might limit the vaporization rate. The major difference between the previous work and that currently undertaken is that the ratio of evaporating to escape area is about 2X greater in the current work.

Although the measurements are not yet complete, the results obtained thus far are plotted in Figure 1. The upper reference curve corresponds to the K pressure observed for decomposition of $KAlO_2$ to the K_2O rich beta-alumina and vapor products. Since $KAlSiO_4$ is formed by reaction of $KAlO_2$ with SiO_2, values of the K pressure are expected to fall below this line. The lower reference curve is the K pressure observed for the decomposition of K_2O poor beta alumina to form Al_2O_3 and vapor products. If decomposition of $KAlSiO_4$ takes place according to reaction (5), the observed K pressure data should fall above this line. Data from a series of heatings are shown. Some of the initial data actually exceeds the upper reference line but decreases as K and O_2 are evaporated from the sample. These points are believed to be due to evaporation of residual impurities (unreacted K_2CO_3) from the sample. As the evaporation process proceeds, there is a tendency for the pressure to decrease with time at constant temperature which is consistent with the traverse of the beta alumina composition toward the K_2O poor phase boundary. In the last series of data (indicated by a dashed curve), it was observed that the K pressure was essentially constant with time even though a large fraction of K_2O has been removed from the sample during this series. At the current stage of the experiment, the K pressure is about a factor of four higher than the K pressure over the $K_2O \cdot 9Al_2O_3$-Al_2O_3 reference curve. About fifty percent of the K_2O content which must be removed before the phase $KAlSiO_4$ disappears from the sample, is still present.

B. Phase Equilibrium Studies (L. Cook)

1. Quench Experiments in the System $K_2O-Al_2O_3-SiO_2$

Determination of subsolidus relations involving $KAlSiO_4$, $KAlO_2$, $K_4Al_2Si_2O_9$, $K_2Si_2O_5$, and K_2SiO_3 was begun, in preparation for study of the K_2O-rich portion of the quaternary system $K_2O-CaO-Al_2O_3-SiO_2$ (see Figure 2). While $K_4Al_2Si_2O_9$ was readily synthesized in the solid state and gave an x-ray powder pattern which agreed well with that reported in the literature (see Ref. 1), considerable difficulty was encountered in synthesizing K_2SiO_3, perhaps explaining the fact that there are apparently no published x-ray data. Removal of carbonate from compositions of 1:1 $K_2CO_3:SiO_2$ appears to be impossible without melting, which further complicates synthesis in view of the pronounced tendency for wetting which these melts have when in contact with platinum. In addition, there appears to be a phase transition in "K_2SiO_3" in the range 600-700 °C. Further attempts will involve complete melting and recrystallization, as the solid state method is seemingly inappropriate. Several combinations of starting materials will then be reacted in order to verify, or perhaps modify, the subsolidus relations depicted in Figure 1, so that detailed thermodynamic analysis of seed/slag interaction may rest on a firm footing.

During the attempt to synthesize K_3AlO_3 (see Ref. 2) for use as an alternative reactant, some unexpected reactions of significance were observed. At temperatures above 1000 °C, potassium carbonate reacts with potassium aluminate to form what is possibly a series of solid solutions (see Figure 2) having rather unusual properties. First, in spite of the fact that both K_2CO_3 and $KAlO_2$ lines are observed in the x-ray powder pattern of 1:1 $KCO_3:KAlO_2$, it does not show signs of melting at temperatures up to 1400 °C. A gray-green color is characteristic, suggesting unusual electronic properties. Additional lines in the powder pattern indicate that the material may have a superlattice if indeed it is single-phase. Further investigation will attempt to determine the nature of this complex seed/aluminate interaction under carefully controlled atmospheric conditions.

2. Quench Experiments in the System $K_2O-CaO-Al_2O_3-SiO_2$

Experiments were conducted to verify the ternary nature of the plane: $CaO-KAlO_2-SiO_2$, which is thought to be a compositional divide of major chemical significance in the quaternary system $K_2O-CaO-Al_2O_3-SiO_2$ (see Figure 3). Specifically, experiments were conducted to determine if the following five reactions proceed to the right as indicated noting that $KAlO_2$ and SiO_2 will combine to form the appropriate phases.

a. $2K_2CaSiO_4 + 2Ca_2Al_2SiO_7 = 3Ca_2SiO_4 + 4KAlO_2 + SiO_2$

b. $K_2CaSiO_4 + CaAl_2Si_2O_8 = Ca_2SiO_4 + 2KAlO_2 + 2SiO_2$

c. $6K_2CaSiO_4 + 2(3Al_2O_3 \cdot 2Al_2O_3) = 3Ca_2SiO_4 + 12KAlO_2 + 7SiO_2$

d. $12K_2CaSiO_4 + 2CaAl_{12}O_{19} = 7Ca_2SiO_4 + 24KAlO_2 + 5SiO_2$

e. $2K_2CaSiO_4 + 2Al_2O_3 = Ca_2SiO_4 + 4KAlO_2 + SiO_2$

Results of the experiments are indicated in Table 1 below. In general, allowing for the possible loss of K_2O, it appears that the plane is ternary, as evidenced by formation of ($KAlO_2$-SiO_2) phases and the presence of Ca_2SiO_4 or related phases. Phase "X" probably contains K_2O. The results of experiment #3 are somewhat in conflict with other results; however, the identity of phase "X'" is not known, and so a judgement cannot be made. Additional experiments will center on the definition of these unknown phases.

Table 1. Experiments in the Plane CaO-$KAlO_2$-SiO_2[1]

	Temperature (°C)	Duration (hours)	Starting Materials	Products[2]
1.	1305	118	(1:1) K_2CaSiO_4/ $Ca_2Al_2SiO_7$	$KAlO_2$(ss)+$K_{1+x}Al_{1+x}Si_{1+x}O_4$ $Ca_2Al_2SiO_7$ + Phase "X"
2.	1305	118	(1:1) K_2CaSiO_4/ $CaAl_2Si_2O_8$	$KAlSiO_4$ + "Ca_2SiO_4"
3.	1287	119	(3:1) K_2CaSiO_4/ ($3Al_2O_3 \cdot 2SiO_2$)	$KAlO_2$(ss)+$K_{1+x}Al_{1+x}Si_{1-x}O_4$+ Phase "X" + Phase "X'"
4.	1305	118	(6:1) K_2CaSiO_4/ $CaAl_{12}O_{19}$	$KAlO_2$(ss)+$Ca_2Al_2SiO_7$ + $K_{1+x}Al_{1+x}Si_{1-x}O_4$+ Phase "X"
5.	1305	118	(1:1) K_2CaSiO_4/ Al_2O_3	$KAlO_2$(ss)+$Ca_2Al_2SiO_7$+ $K_{1+x}Al_{1+x}Si_{1-x}O_4$+ Phase "X"

[1] Specimens were sealed in Pt capsules and quenched in liquid N_2. Invariably capsules with K_2CaSiO_4 swelled extensively during the experiments, and so some loss of K_2O may have occurred.

[2] Phase "X" is an unidentified phase, probably related to Ca_2SiO_4 with major lines at 1.98, 2.19, 2.60, 2.74, and 2.78 A.

Phase "X'" has major lines at 3.05 and 3.11 Å.

In Table 2 are given results of experiments designed to explore the phase equilibrium properties of the more K_2O-rich portion of the quaternary system K_2O-CaO-Al_2O_3-SiO_2. In these experiments, as well as those in Table 1, the compound K_2CaSiO_4 has been employed extensively as a starting material: its reported melting point (Ref. 3) is relatively high, in excess of 1600 °C, and hence its region of stability is of interest. As Table 2 shows, however, K_2CaSiO_4 is present only in results of experiment #7. This experiment suggests existence of a compound between $KAlO_2$ and K_2CaSiO_4. The identity and stability of this compound will be investigated further. Phase "Z" in experiment #8 may be a compound intermediate between K_2CaSiO_4 and Ca_2SiO_4. The results of experiment #9 reaffirm compatibility of $KAlO_2$ and CaO (Ref. 4).

Table 2. Experiments in the K_2O-rich Part of the System K_2O-CaO-Al_2O_3-SiO_2[1]

	Temperature (°C)	Duration (hours)	Starting Materials	Products[2]
6.	1287	119	(1:1) K_2CaSiO_4/ $KAlSiO_4$	$Ca_2Al_2SiO_7$ + $KAlSiO_4$ + $K_{1+x}Al_{1+x}Si_{1-x}O_4$ + Phase "Y"
7.	1287	119	(1:1) K_2CaSiO_4/ $KAlO_2$	$KAlO_2$ + K_2CaSiO_4 + Intermediate phase
8.	1305	118	(1:1) K_2CaSiO_4/ Ca_2SiO_4	Glass + Phase "Z"
9.	1287	119	(1:1) $KAlO_2$/CaO	$KAlO_2$ + CaO

1. See Footnote 1, Table 1.

2. Phase "Y" has major lines at 2.14, 3.42, and 4.27 Å.
Phase "Z" has a major line at 2.97 Å and numerous weaker lines.

Figure 4 has been constructed to show the rather extensive stability of the compound $Ca_2Al_2SiO_7$. It coexists with compounds under both relatively high K_2O pressures (with $KAlO_2$ ss) and at relatively low K_2O pressures and high silica contents (with $KAlSi_2O_6$).

Plans:

- Vaporization measurements on the K_2O-Al_2O_3-SiO_2 system will be completed to as low a K_2O composition as practical.
- Vaporization measurements on K_2O containing compositions in selected sections of the K_2O-Al_2O_3-SiO_2-CaO system will be started.
- Verify existence of $K_2CO_3/KAlO_2$ solid solutions and determine their nature.
- Confirm proposed subsolidus relations in K_2O-Al_2O_3-SiO_2.
- Identify unknown phases in K_2O-CaO-Al_2O_3-SiO_2 system and determine their stability.
- Prepare quaternary melts for vaporization studies.

References:

1. L. K. Yakovlev, Russ. J. Inorg. Chem., 10[12], 1459 (1965).

2. A. Bon, C. Gleitzen, A. Courtois and J. Protas, C. R. Acad. Sci., Ser. C., 278[11], 785 (1974).

3. G. W. Morey, F. C. Kracek and N. L. Bowen, J. Soc. Glass Tech., 14, 149 (1930).

4. L. T. Brownmiller, Am. J. Sci., 5th Ser., 29, 268 (1935).

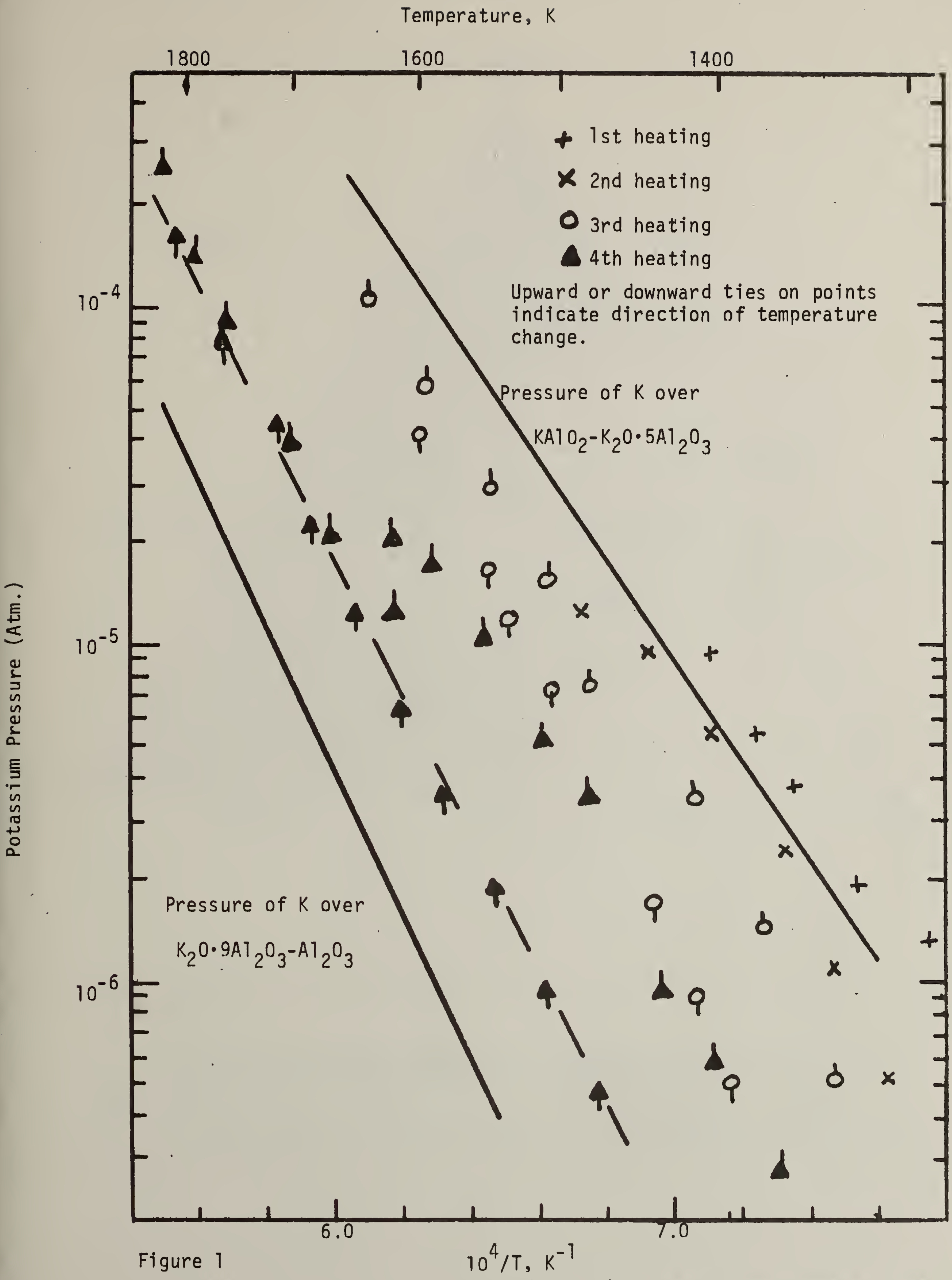

Upward or downward ties on points indicate direction of temperature change.

Figure 1

Selected K pressures over orthorhombic $KAlSiO_4$, leucite and beta alumina showing decrase in pressure possibly because of shift in composition of beta alumina.

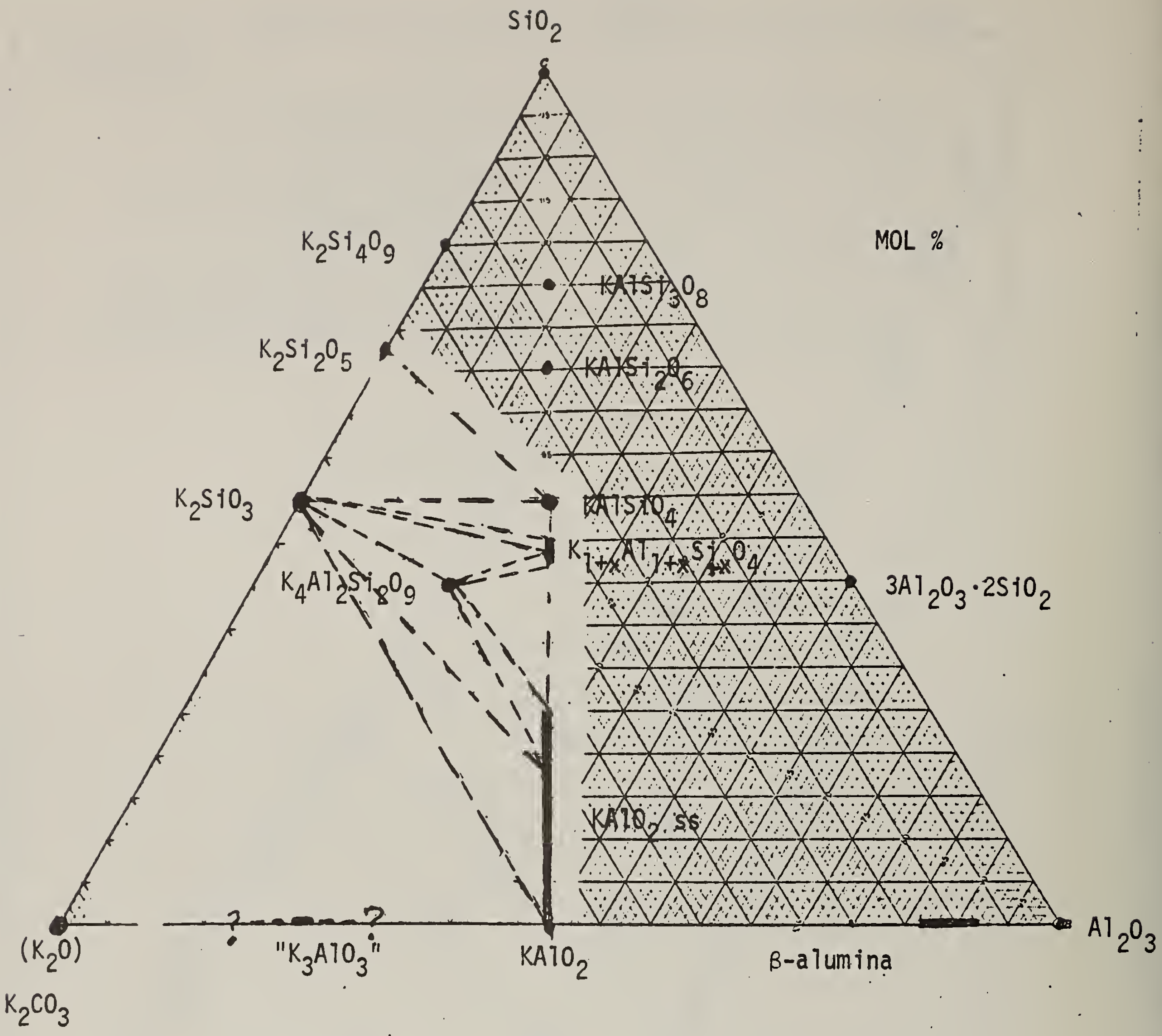

Figure 2

Proposed tie-line distribution in the K_2O-rich part of the system K_2O-Al_2O_3-SiO_2. (Modified after H. P. R. Frederickse, T. Negas and S. J. Schneider, Development; Testing and Evaluation of MHD-Materials, NBS Quarterly Report prepared for U.S. Energy Research and Development Administration under Contract No. E(49-189-1230), July-September 1975, p. 30).

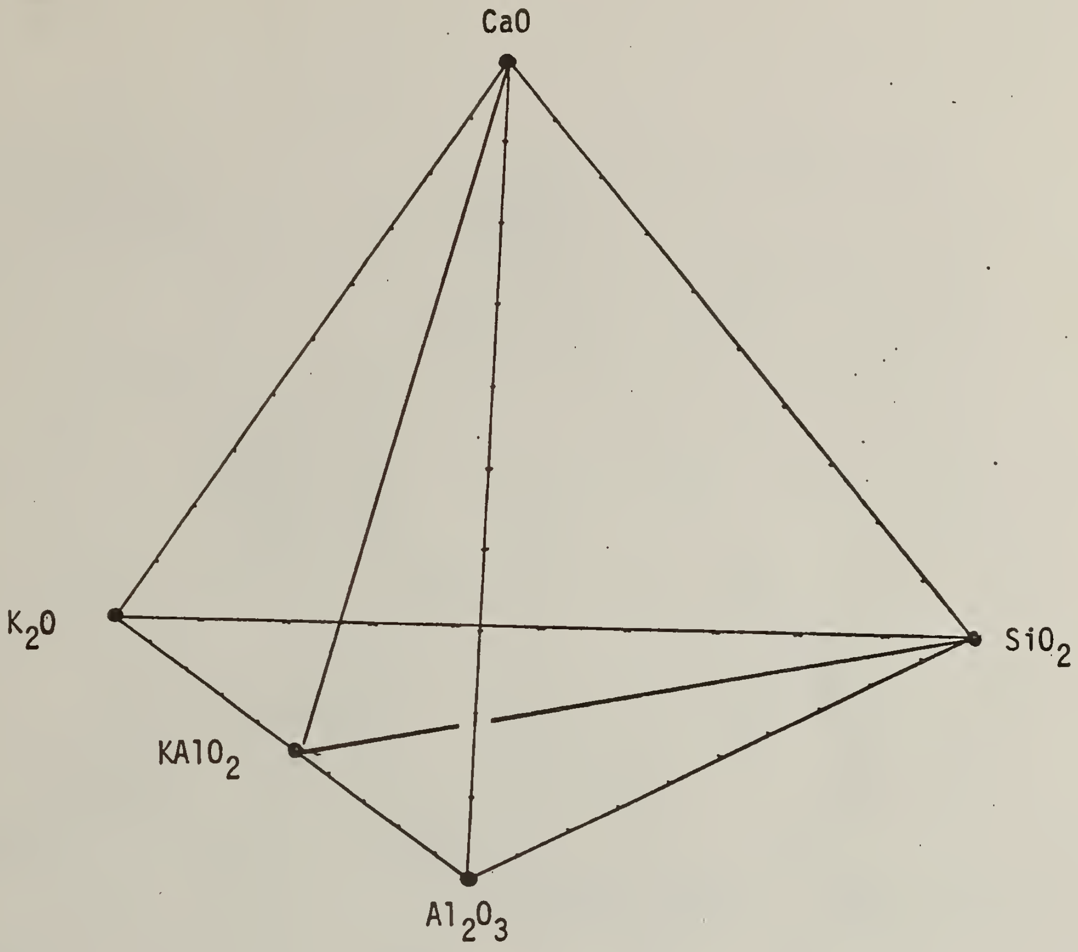

Figure 3

Compositional divide formed by the tornary plane $KAlO_2$-SiO_2CaO in the quaternary system K_2O-Al_2O_3-SiO_2-CaO.

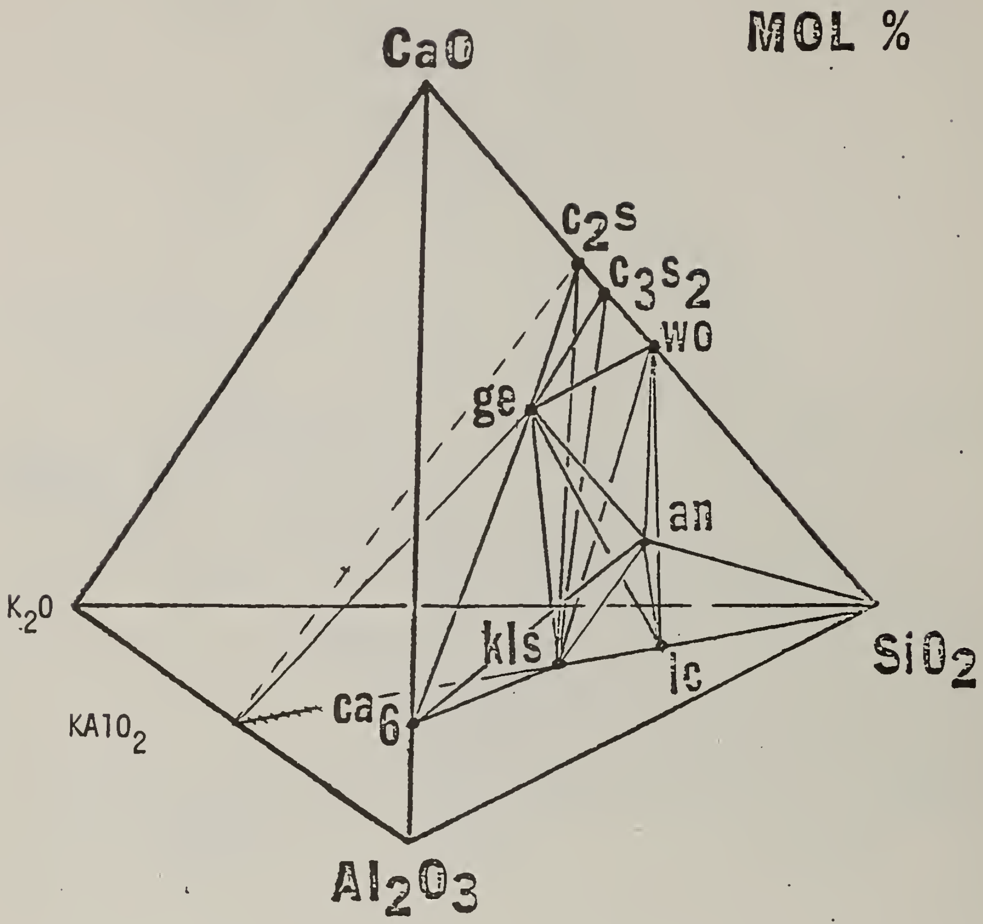

Figure 4

Compatibility of gehlenite ("ge" = $Ca_2Al_2SiO_7$) with other phases in the quaternary system. "c_2s" = Ca_2SiO_4; c_3s_2 = $Ca_3Si_2O_7$; "WO" = $CaSiO_3$; "an" = $CaAl_2Si_2O_7$; "kls" = $KAlSiO_4$; "lc" = $KAlSi_2O_6$; ca_6 = $CaAl_{12}O_{19}$.

2. Electrical Conductivity and Polarization (W. R. Hosler)

Progress

a. Electrical Conductivity of $YCrO_3$.

The dependence of the electrical conductivity of $Y_{.95}Ca_{.05}CrO_3$ on oxygen pressure in the range of pressures from 10^0 to 10^{-6} atmospheres have been completed for temperatures from 1300°C to 1600°C. In order to obtain high density $YCrO_3$, it is necessary to sinter it in a highly reducing atmosphere at about 1700°C. This atmosphere may be forming gas (5% H_2 - 95% N_2) which results in a low pressure of O_2 of 10^{-14} to 10^{-15} atmospheres. Material produced under these conditions has a high density (98% theoretical) and is very hard. Subsequent oxidation renders the material much softer and it sometimes contains hair line cracks. The material with 5% Ca added is still single phase when oxidized but the oxygen take up must cause enough change in the lattice parameters in certain areas to cause a stress build up with the resultant physical sample degradation. This aspect of the problem is being investigated by the Crystal Chemistry Section of CMR at NBS. The dimensional changes associated with this effect are very small and cannot account for the increase in conductivity noted in the last quarterly report for 1600°C temperature point in an atmosphere of air. The continual drift upward in conductivity noted for the 1600°C point in air was not evident at any temperature in 900 and 2 ppm oxygen in nitrogen.

The sample holder has been revised using 0.25 mm molybdenum wire instead of platinum. The wire leads are anchored in the sample with platinum. The phase diagram of Pt-Mo shows a eutectic mixture at about 25 atomic % platinum and at a temperature of 2080°C. The conductivity vs. pressure measurements will be made using a maximum temperature (1600°C) well below this eutectic point. No reaction is expected. In the previous measurements in the oxygen pressure range of 10^{-7} to 10^{-15} ppm O_2, the platinum wire leads failed. The platinum contacts in the sample always remained intact, however. These measurements at the low oxygen pressure will be made as soon as the oxygen sensor necessary for measuring these low pressures is repaired.

b. Corrosion of $YCrO_3$ in Slag

In the last quarterly report, the results of a test on an electrochemical cell composed of $YCrO_3$ electrodes and Bow NH slag with 20% K_2SO_4 added were reported. This test was carried out at 1343°C and resulted in considerable cathode reaction but with not much reaction at the anode. A new cell has been constructed and tested using the same materials (Bow NH slag with 20% K_2SO_4 electrolyte and $Y_{.95}Ca_{.05}CrO_3$ electrodes) but with a slightly different configuration. This cell contains 3 electrodes, two of which are active (anode and cathode at each end of the cell) and one which is passive (center of cell) which carries no current. This allows for direct measurement of the potential distribution along the length of the cell i.e. for potentials between anode and reference and between reference and cathode. No polarization should result on the reference electrode since no current enters or leaves at this point. There may be degradative chemical reactions, however, at the reference electrode not associated with the transport of charge. These measurements were carried out at 1254°C and with a power supply providing a constant DC voltage source of 118 volts. The results are shown in Figure 1. Initial current was about 75 ma which would correspond to approximately 0.5 amp/cm^2 current density at the electrode slag interface. This current drops off to about 20% of its original value or 15 ma in the first 20 minutes of cell operation and finally down to about 8 ma after the total test time of 3 hours and 50 minutes. In the initial 20 minute period, the anode to reference voltage increased to 110V i.e. within 8 volts of the total applied potential while the reference to cathode voltage dropped to about 8 volts. It is obvious that a large polarization potential has built up at the anode. This is most likely due to the zone near the anode that is silica rich or depleted in movable positive ions such as iron and potassium. On the other hand, positive ion transport toward the cathode lowers the potential barrier there, as well as the bulk conductivity of the slag. This effect has been observed before using other materials (1,2,3) and is certainly a contributing factor in the cathode electrode segment voltage nonuniformities observed in some of the AVCO tests reported in the 16th Symposium on Engineering Aspects of MHD held at the University of Pittsburgh in May 1977.

Electrical conductivity measurements on Bow NH slag discussed later in this section of the report under Slag Electrical Conductivity (Part C) indicates that a sizeable fraction of the charge carried in slag is transported by ions. The basic question in MHD electrode materials is: How can this mass transport and its associated electrochemical effects be handled? One interesting aspect of the situation is to ascertain if any of the resulting electrochemical effects are reversible and under what conditions. Preliminary indications from the AVCO generator experiments show that the effects causing cathode voltage nonuniformities can be reduced by running the channel at no load (open circuit) for a period of time. An electrochemical cell for investigating the reversibility of these effects is under construction.

c. Slag Electrical Conductivity

The electrical conductivity of Bow NH slag with 20% K_2SO_4 added to the melt has been completed. Figure 2a and b show radiographs of the crucible containing the slag before and after the experiment. No observable physical change has taken place during the experiment. Figure 3 shows the conductivity data as a function of temperature. All data was taken at a partial pressure of oxygen of 2 x 10^{-6} atmospheres. The temperature from which the slag was furnace quenched to 900°C is indicated on the graph. The conductivity data at reduced oxygen pressure is not quite so quench temperature dependent as that data for the conductivity in air shown in the last quarterly report (July-Sept. 1979). The magnitude and the general trend is the same, however. There appears to be two crystalline phases contributing to the conductivity. In the reduced O_2 pressure experiment, a break in the conductivity curve occurs near 1160°C for all data; the break becoming more pronounced for the runs where the sample is quenched to 900°C from soak temperatures above 1400°C. All data shown on the graph is taken with increasing temperature after being quenched to 900°C and cooled slowly to the lower temperature (∿500°C). The data below 800°C may be affected by cracks in the slag body formed by quenching to 900°C and subsequent cooling to lower temperatures. Cracking appears to be more severe in those samples with the K_2SO_4 added. It would be interesting to see how the coefficients of thermal expansion for these seeded and unseeded slags differ. X-Ray diffraction measurements (courtesy of H. Parker, Center for Materials Science, Solid State Chemistry Group) show that the phase composition below 1180°C is a kalsilite like phase (probably $KAlSiO_4$) and spinel (Fe_3O_4) for that material quenched from 1426°C. This kalsilite like phase was not detected in the slag measured in an air atmosphere and quenched from nearly the same temperature (1420°C). The spinel (Fe_3O_4) was detected in the sample measured in air. The interesting and unusual aspect is that the slag conductivities for Bow NH slag with and without seed and measured in air and in an atmosphere of 2×10^{-6} O_2 partial pressure are the same as a function of temperature above 1400°C. If the potassium ion conductivity is the predominant mechanism for charge transport, above 1400°C, the samples containing added K_2SO_4 should have a higher conductivity. Chemical analysis for K and S of the Bow NH slag with 20 wt.% K_2SO_4 added to the melt before and after the electrical measurement (2×10^{-6} atmos O_2) are given in Table 1.

Table 1

	% K	% S
Before conductivity measurement	6.34	.022
After conductivity measurement	5.99	0.12

The magnitude of sulfur detected in each case was below the accurate limits of detection. It apparently leaves during initial melting of the slag and K_2SO_4 mix. The reason for the discrepancy between the amount of K added (9%) and that detected in the analysis is unknown. If the conduction mechanism is predominantly electronic above 1400°C and due to the iron ion ratio Fe^{+2}/Fe^{+3} one would expect a higher conductivity in that sample measured in a partial pressure of oxygen of 2×10^{-6} atmospheres. Johnson (4) has reported an Fe^{+2}/Fe^{+3} ratio at 1450°C of 1.6 for an oxygen pressure of 10^{-6} atmospheres and of 0.13 for an air atmosphere. This gives a ratio change of near 13 which should be reflected in the conductivity if there is exchange between the iron ions of different valence. The measured conductivity of the slag above 1400°C is not likely to be due to oxygen ions since the conductivity is not oxygen pressure independent. The slag sample at high temperature is a disordered structure (molten) and it is not surprising that the electron exchange is small between Fe^{+2} and Fe^{+3}. Simnad, Derge, and George (5) in transport measurements on iron in silicate slags conclude that the transport number of the iron ions Fe^{+2} is one and therefore that the current is being carried almost completely by these ions. The ionic radius of K^{+} is large (1.33A) while that of Fe^{+2} and Fe^{+3} is 0.74A and 0.64A, respectively. This difference in ionic radii coupled with the difference in ionic charge may make the iron ion the predominant charge carrier in the molten slag.

The relative amounts of Fe^{+2} to Fe^{+3} then would have a secondary effect on the electrical conductivity. The total iron content, however, would affect the magnitude of the conductivity. This coorelation was pointed out earlier by Bates (6) in his analysis of early slag conductivity work done by Frederikse and Hosler (7).

d. Other Activities

1. During the course of channel proof tests in preparation for the 3rd Joint US-USSR Materials Test in the U.02 MHD facility in Moscow, the electrical conductivity of $Sr_{0.9}La_{0.1}Zr_{0.7}Cr_{0.3}O_3$ was measured as a function of temperatue and oxygen pressure. This material was prepared by A. T. Research and no details were given on its preparation. The data was presented in quarterly report Oct-Dec. 1977 to DoE. An inquiry was received from Dr. H. Shapiro from T. R. W. concerning this material with regard to its large range showing a positive temperature coefficient of resistance in an air atmosphere. Another sample was sent from T. R. W. and the conductivity measured during this reporting period. The resulting data is shown in Figure 4. The range showing a positive temperature coefficient of resistance is reduced considerably and shows a hysteresis effect with increasing or decreasing temperature indicative of a reversible phase change.

2. During the week of October 8th, W. Hosler attended the joint 16th International Thermal Conductivity Conference and the 7th International Thermal Expansion Symposium held in Chicago at the IIT Research Institute on Nov. 7-9.

3. On December 5 and 6, W. R. Hosler participated as a panel member for Materials in the review of the DoE sponsored work of MERDI at Butte, Montana. The review was held at Montana State University, Bozeman, Montana.

References

(1) Electrochemical Effects in Simulated Slag Flow
W. Capps, D. A. Kauffman, and W. R. Hosler, Quarterly Report for the period April-June 1978 to DoE under contract No. EA-77-A-01-6010.

(2) Discharge Characteristics of Slagging Metal Electrodes
J. K. Koester and R. M. Nelson, 17th Symposium on Engineering Aspects of MHD. Stanford University, Stanford, California. March 27-29, 1978.

(3) Electrochemical Corrosion of MHD Electrodes in Slags
L. D. Cadoff, D. B. Rossing, and H. D. Smith, 17th Symposium on Engineering Aspects of MHD, Stanford University, Stanford, California. March 27-29, 1978.

(4) Oxidation - Reduction Equilibria in Iron Containing Glass
W. D. Johnson, Journal of Am. Cer. Soc., Vol. 47, No. 4, April 1964.

(5) Ionic Nature of Liquid Iron - Silicate Slags AIME Transactions
M. T. Simnad, G. Derge, and I. George, Journal of Metals, <u>200</u>, p. 1386, Dec. 1954.

(6) Private communication.

(7) Electrical Conductivity of Coal Slag
H. P. R. Frederikse and W. R. Hosler, Journal of American Ceramic Society, Vol. <u>56</u>, No. 8, August 1973.

Plans

The electrical conductivity of $YCrO_3$ doped with 5% Ca on the Y site in the oxygen pressure range of 10^{-6} to 10^{-15} atmospheres will be completed. Experimental difficulties here have been largely overcome and the outcome measurements may depend on the physical stability of the material upon going from an oxidizing to a reducing atmosphere.

The work on the slag electrical conductivity will continue. A decision must be made whether to continue with the Bow NH slag (doping or increasing iron content, etc.) or begin to study extensively the conductivity mechanisms in low iron high calcium slag (Rosebud).

The electrochemical experiments involving slag and electrode materials will continue particularly with respect to the possible reversibility of these effects or with respect to the time limits involved when electrochemical reactions degrade conductivities far enough to limit usefulness.

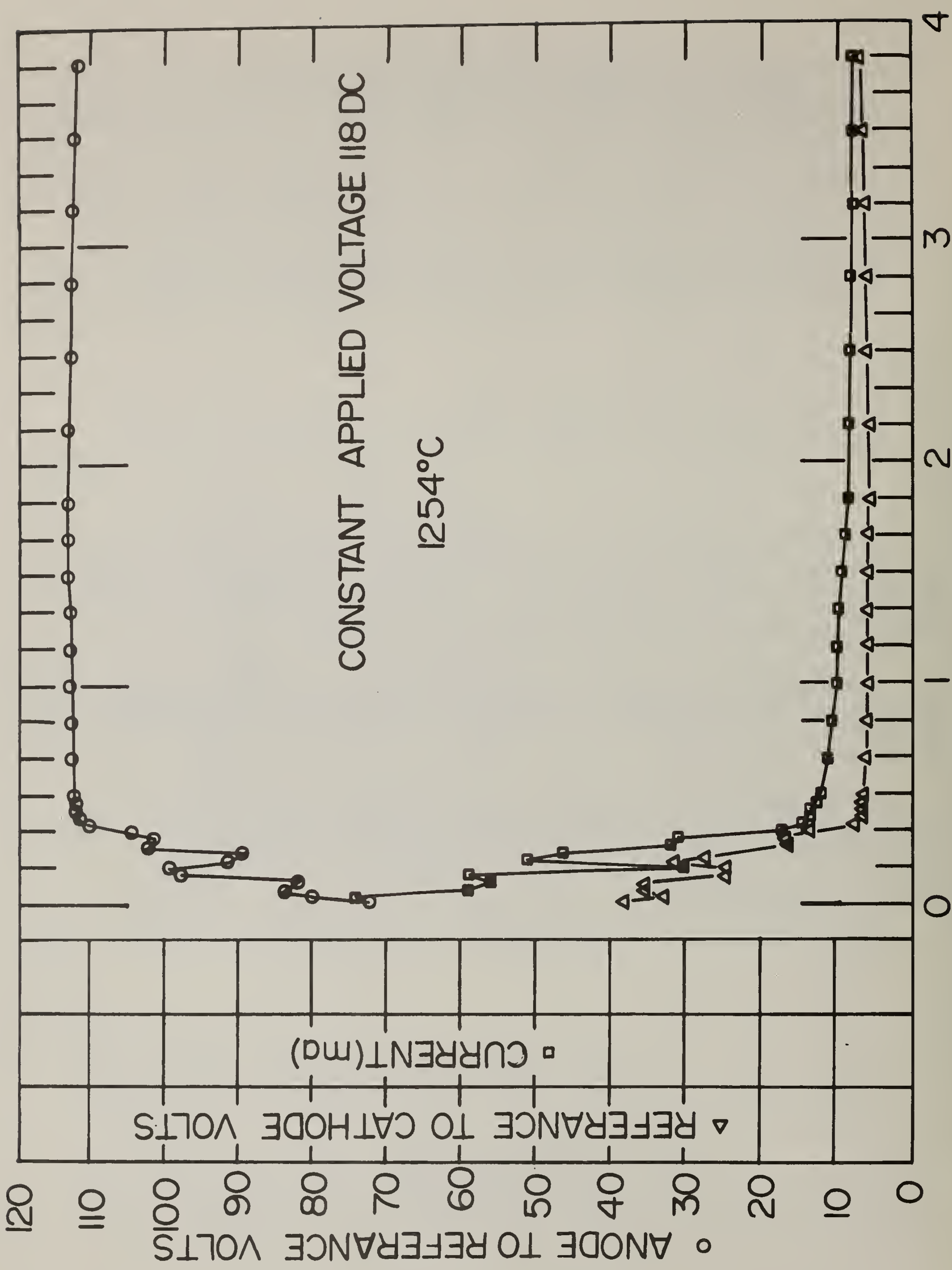

Figure 1. Time vs. voltage relationships in an electrochemical cell of $Y_{.95}Ca_{.05}CrO_3$ in a slag electrolyte with added K_2SO_4.

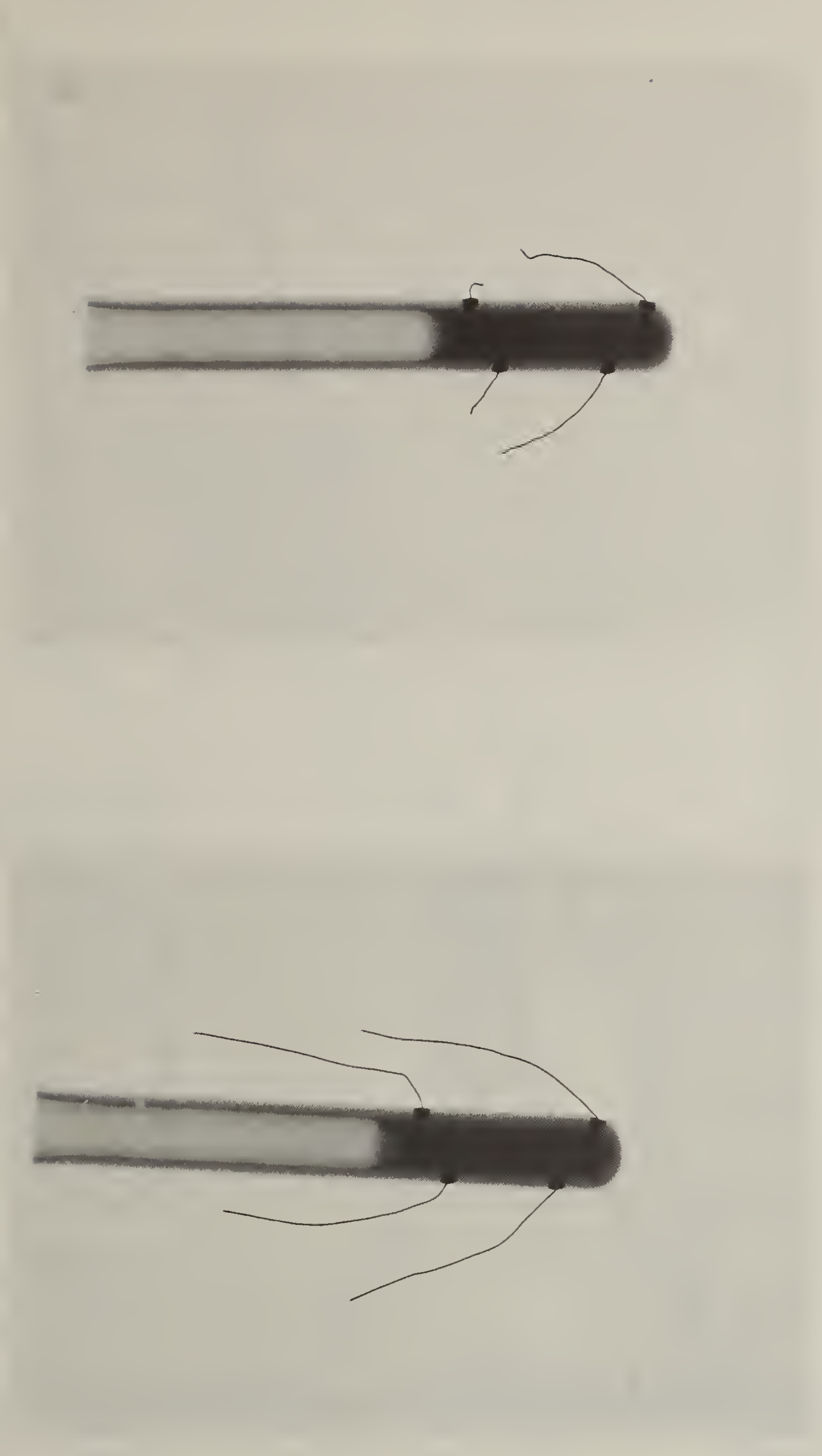

Figure 2. Radiograph of crucible showing slag fill and electrode configuration before (a) and after (b) electrical conductivity measurements.

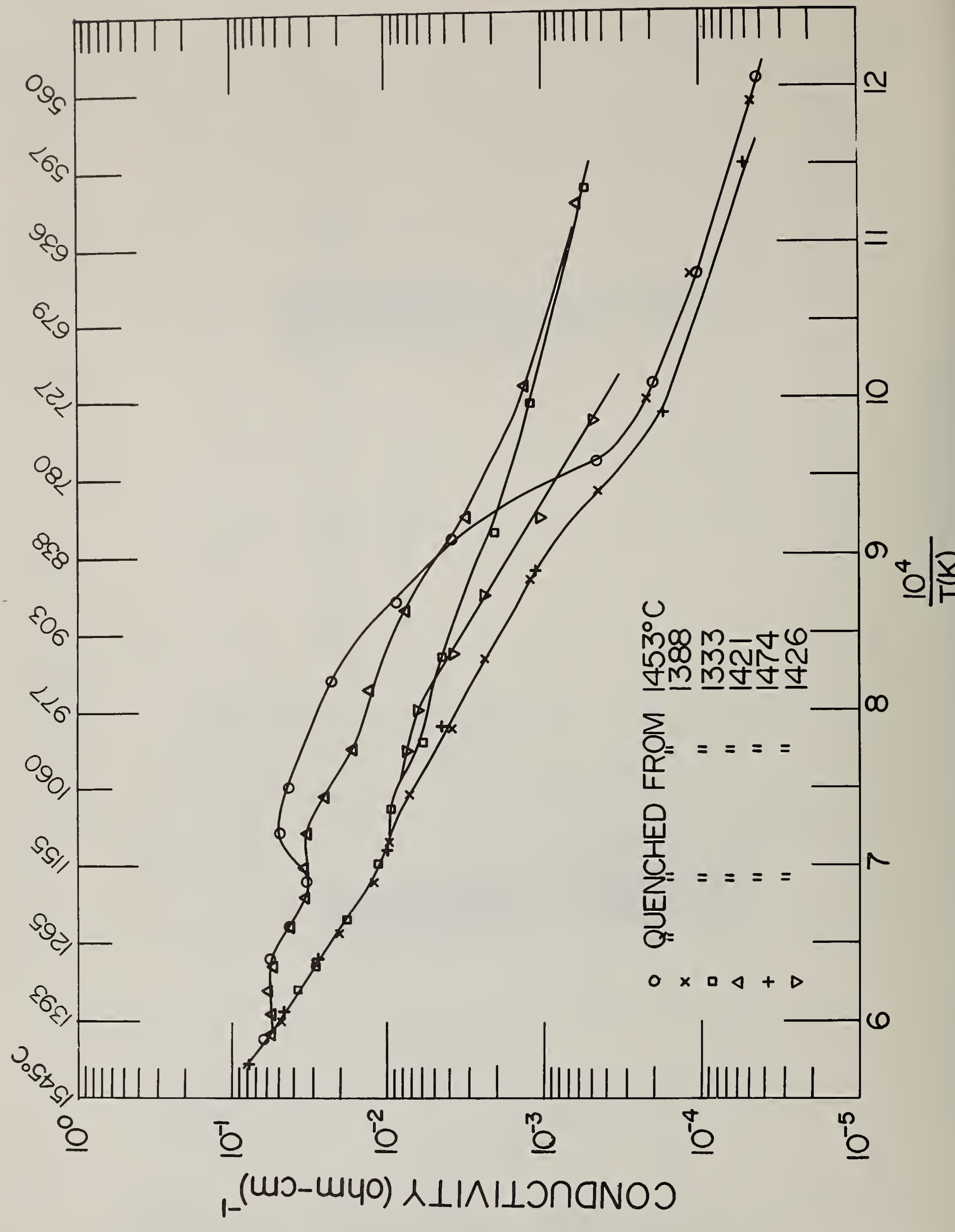

Figure 3. Electrical conductivity of Bow NH slag with 20% K_2SO_4 added to the melt. All data was taken in 2 x 10^{-6} O_2 atmospheres in N_2 and with increasing temperature after being quenched to 900°C from the equilibration temperatures indicated on the graph.

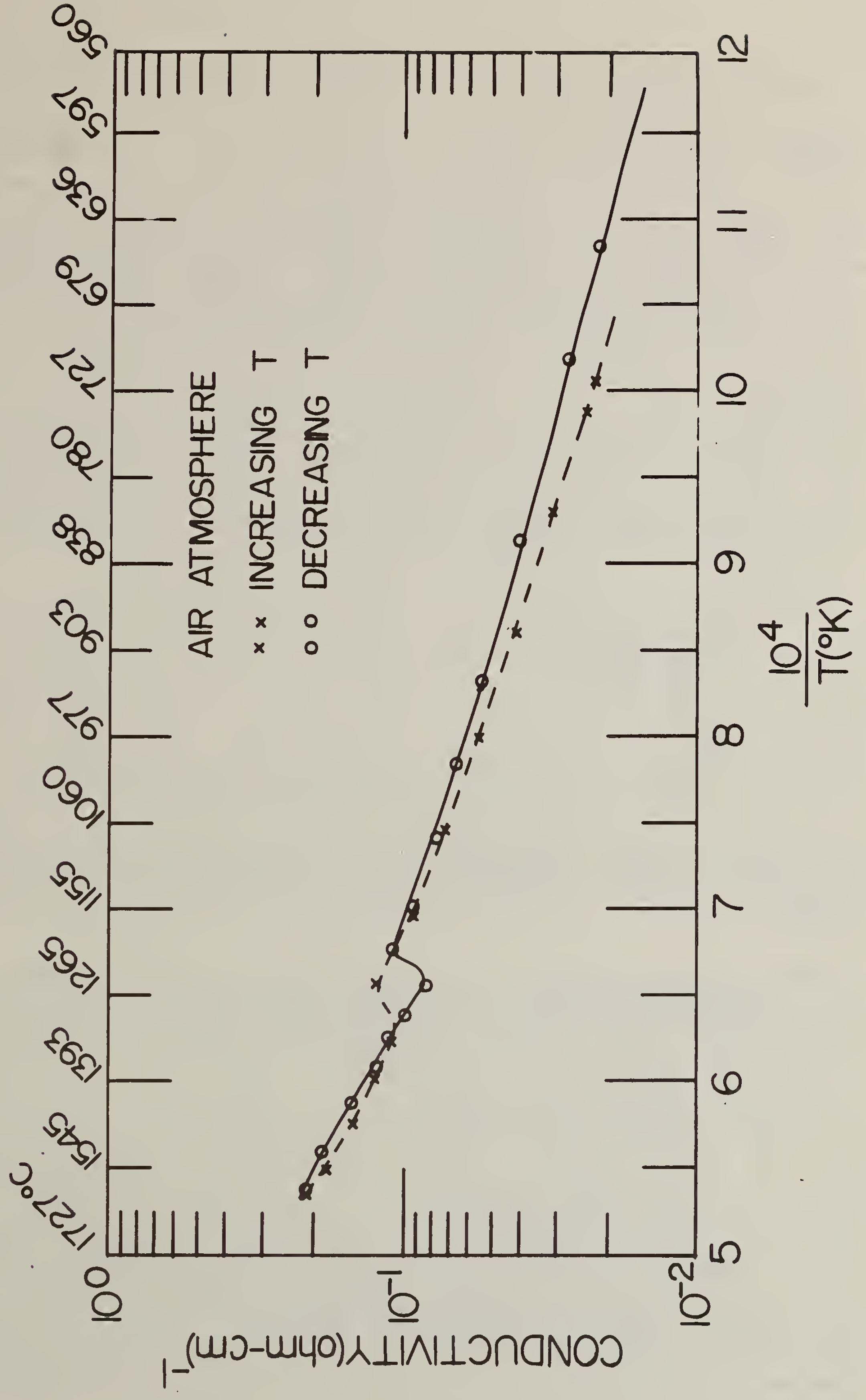

Figure 4. The electrical conductivity of $Sr_{0.9}La_{0.1}Zr_{0.7}Cr_{0.3}O_3$ as a function of temperature for increasing and decreasing temperatures.

3. Corrosion of Downstream MHD Components (J. Smit, and C. D. Olson)

Progress: Type 304 stainless steel tubular specimens were exposed to a seeded oxygen-propane fueled hot gas stream under varied conditions and then analyzed by SEM and EDX techniques. Total exposure time to the hot gas stream was 4 hours with the first 25 minutes of this period being used to seed the gas stream with 250 g of a mixture of 80% by weight K_2CO_3 with 20% by weight K_2SO_4. Six stainless steel 304 specimens were tested under these general conditions. Three of the tubular specimens were exposed to an oxygen rich gas stream environment at tube temperatures of 400° C, 500° C and 590° C, respectively. The remaining three samples were exposed to a fuel rich gas stream environment at 400° C, 500° C and 590° C. Specimen temperatures were maintained at the desired value by internal air cooling and were monitored through a Pt/Pt 10% Rh thermocouple welded into the specimen wall. In the vicinity of the test specimen the gas stream temperature was maintained at approximately 1300° C as monitored through a Pt/Pt 10% Rh thermocouple. The fuel rich and the oxygen rich states were accomplished by varying oxygen to propane flow rate ratios.

To reduce external contamination of the samples and hydration of the K_2CO_3 in the coatings formed during seeding of the hot gas stream, the samples were removed from the test rig upon cool down to about 40° C and potted immediately in epoxy. Metallographic specimens were then prepared from sections of the stainless steel tube taken approximately 10 mm from the midpoint position in the hot zone. The speicmens were then ground and polished using nonaqueous media. All samples were stored in evacuated desiccators until ready for SEM/EDX analysis.

On all specimens a compact deposit formed on the surface facing the gas stream. A powdery deposit, probably from the fume, formed on the trailing surface. At the boundary between the two, a thicker drip zone formed.

On the specimens exposed to the oxygen rich gas stream the leading surface deposit, which varied with temperature (thickest at 400° C) ranged from 1.7 mm to 0.8 mm. The trailing surface deposit was fairly uniform at about 0.2 to 0.3 mm, Figures 1, 2 and 3.

EDX analysis shows high concentration of potassium with traces of sulfur throughout the bulk of the salt deposit, however, the top layer of the salt deposit is high in sulfur (K_2SO_4). In previous tests using only K_2SO_4, a layered deposit was formed on the specimens. However, with the K_2CO_3/K_2SO_4 charge, layering did not occur but small potassium rich nodes were found in a matrix of potassium and sulfur. Figure 4, specimen temperature 400° C shows these small nodes. Again, Figure 5, specimen temperature 500° C, shows the potassium rich nodular formations. In the 590° C sample, Figure 6, the nodes are not predominate and a more even surface can be observed. An explanation for the difference in the coating would be that two different salts with melting points varying by 178° C would show areas of incongruent melting. However, at the edge of the coating, it is possible that the hot gas stream volatilized the K_2CO_3 leaving behind a greater concentration of sulfur than potassium in the form of K_2SO_4.

The corrosion band area on the 304 stainless steel increases with increasing temperature. The variation in corrosion can be observed in the comparison of Figure 7, specimen temperature 500° C with Figure 8 specimen temperature 590° C. SEM/EDX analysis of both samples, Figures 7a-7g and Figures 8a-8j, indicate metal corrosion and metal cation migration, however, the 590° C specimen shows the corrosion picture more vividly.

SEM/EDX analysis seems to indicate that preferential leaching of the metal cations from the bulk materials (304 stainless steel) is found in a somewhat orderly fashion. The analysis shows that, moving from the stainless steel bulk material to the salt deposit, a high chrome concentration area is found along the edge of the tube and below the surface of the tube top. Areas of high nickel concentration are found within the high chrome concentration matrix while areas of high iron concentration are found next to the salt. Figures 9a-9f show that the iron is found in areas of high potassium concentration a good distance away from the reaction interface region of the stainless steel/salt deposit. Figures 10a-10c again show iron well away from the reaction zone.

In a fuel rich hot gas stream, a thin, 0.6 to 0.8 mm, as compared to the oxygen rich environment, salt deposit was formed. As noted in the oxygen rich series these samples also exhibited decreasing thickness with increasing temperature. In contrast to the oxygen rich specimen the fume deposit, 0.4 to 0.7 mm (the layer on the under side of the tube), was heavier. However, it also decreased with temperature, Figures 11, 12 and 13.

As in the oxygen rich test samples the fuel rich samples also exhibited reaction zone areas. Again, these areas showed increased activity in corrosion with increased sample temperature. Figure 14, specimen temperature 500° C and Figure 14, specimen temperature 590° C show areas of corrosion at the stainless steel/salt interface with areas of high metal cation concentration. However, the reaction areas do not seem to be as great under the fuel rich conditions as compared to the oxygen rich conditions.

As noted by SEM/EDX analysis, Figures 14a-14g and Figures 15a-15g, the edge of the stainless steel bulk material contains regions of high chrome concentration are found next, with iron and potassium in the salt deposit adjacent to the stainless steel. The salt deposit seems to contain more sulfur than in the oxygen rich cases, but both have a crust of potassium and sulfur in high concentration on the top of the salt layer.

Both systems, oxygen rich and fuel rich, show evidence of metal corrosion. However, the fuel rich system seems to show less evidence of damage to the bulk stainless steel. Both system also seems to indicate the same metal cation movement from the bulk stainless steel towards the salt deposit.

<u>Stainless Steel Reference Specimen</u> - As with most analytical techniques, reference samples are used to check some stage of the analysis. At the present time a randomly selected sample type 304 stainless steel that has been cleaned, cut and polished has been used to check outer edges or surfaces for areas where corrosion would most likely occur. A general overview of the tube (Figure 16) would seem to indicate that the 304 stainless is very clean and uniform on the outer edges. However, Figures 17 and 18, shows that in the manufacturing, rough surfaces, i.e., holes and put areas, can occur. These areas would be more susceptible to a corrosion process and promote deterioration of the surface under hot plasma and seeding conditions. Therefore, not all areas analyzed for pits and holes are necessarily due to the corrosion process. EDX analysis shows that traces of sulfur are already present in the matrix. No other inconsistences such as areas of high chrome concentration or high iron concentration are found in the metal, but rather a uniform distribution of chrome, iron and nickel is found throughout the 304 stainless steel.

<u>Plans</u>: Specimens of type 304 stainless steel will be evaluated at 100 hours exposure to a hot gas atmosphere, fuel rich and oxygen rich, with seeding of a salt every 24 hours. Samples will then be anlayzed using SEM/EDX to establish corrosion and leaching of metal cations.

A program will be initiated using type 316 stainless steel tubular specimens under the same general conditions that have been established in running the type 304 stainless steel samples.

Fig. 1. Section of Type 304 stainless steel tubing after exposure to K_2CO_3/K_2SO_4 seeded oxygen rich hot gas stream. Note formation of thick deposit, 1.7 mm, on upper surface and thin powdary deposit on lower surface. Tube temperature 400°C. 6 X.

Fig. 2. Section of Type 304 stainless steel tubing after exposure to K_2CO_3/K_2SO_4 seeded oxygen rich hot gas stream. Note formation of thick deposit, 1 mm on upper surface. Tube temperature 500°C. 6 X.

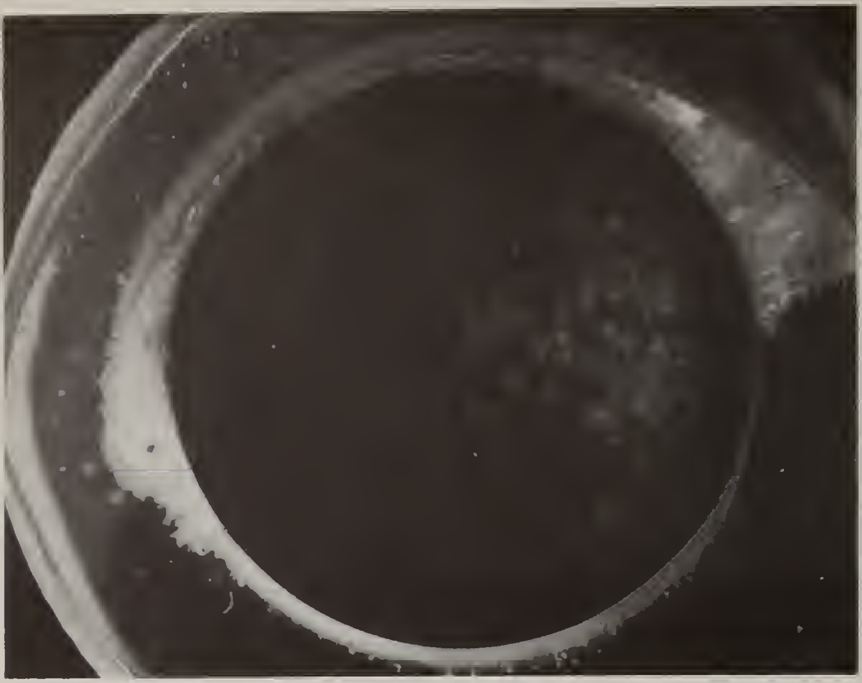

Fig. 3. Section of Type 304 stainless steel tubing after exposure to K_2CO_3/K_2SO_4 seeded oxygen rich hot gas stream. Note formation of thinner deposit on upper surface. Tube temperature 590°C. 6 X.

Fig. 4. SEM micrograph, 200 X, of small, high potassium concentration nodes in the salt deposit. Specimen temperature 400°C; gas stream oxygen rich.

Fig. 5. SEM micrograph, 200 X, of small, high potassium concentration nodes in the salt deposit. Specimen temperature 500°C; gas stream oxygen rich.

Fig. 6. SEM micrograph, 200 X, of salt deposit showing absence of high potassium concentration nodules. Specimen temperature 590°C; gas stream oxygen rich.

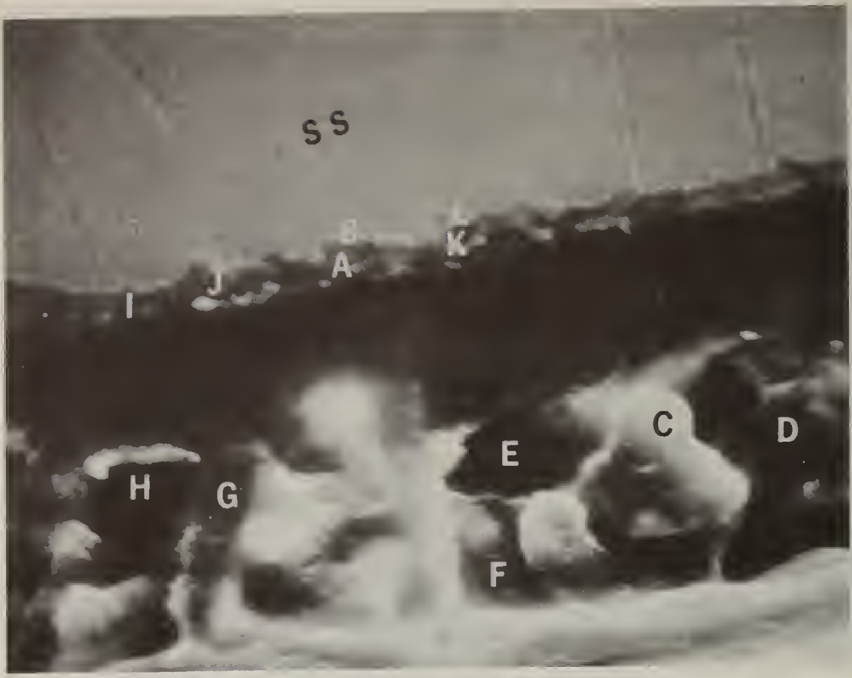

Fig. 7. SEM micrograph, 2000 X, of stainless steel-salt deposit reaction zone. Lettered regions correspond to labeled EDX spectra, figures 7a through 7f. Specimen temperature 500°C; gas stream oxygen rich.

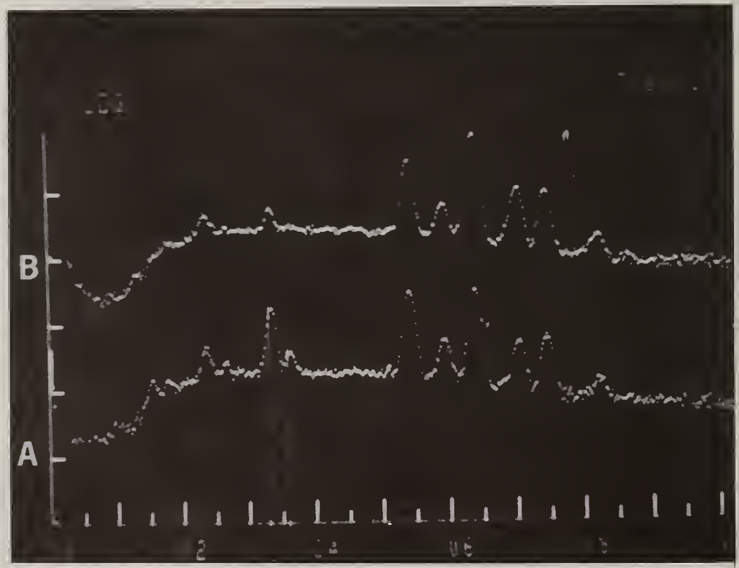

Fig. 7a. EDX spectra of regions A and B of figure 7 showing high Cr concentration area.

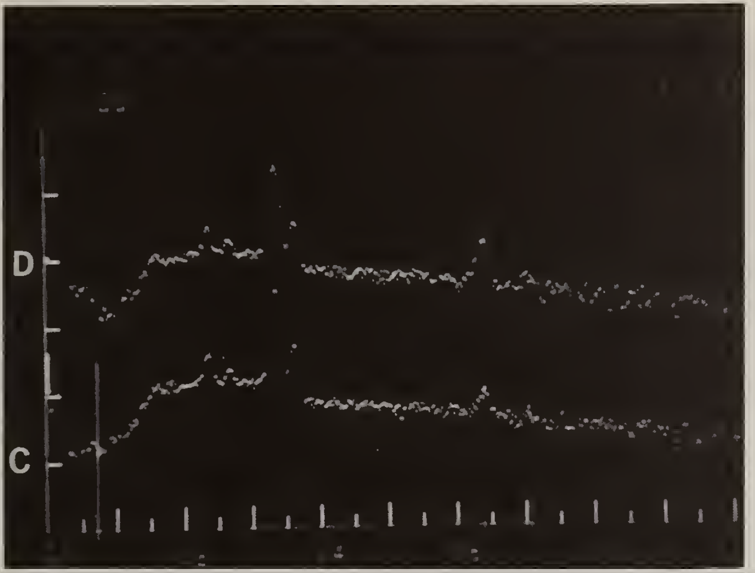

Fig. 7b. EDX spectra of regions C and D of Fig. 7 showing region of high potassium concentration associated with Fe in the salt region of the corrosion area.

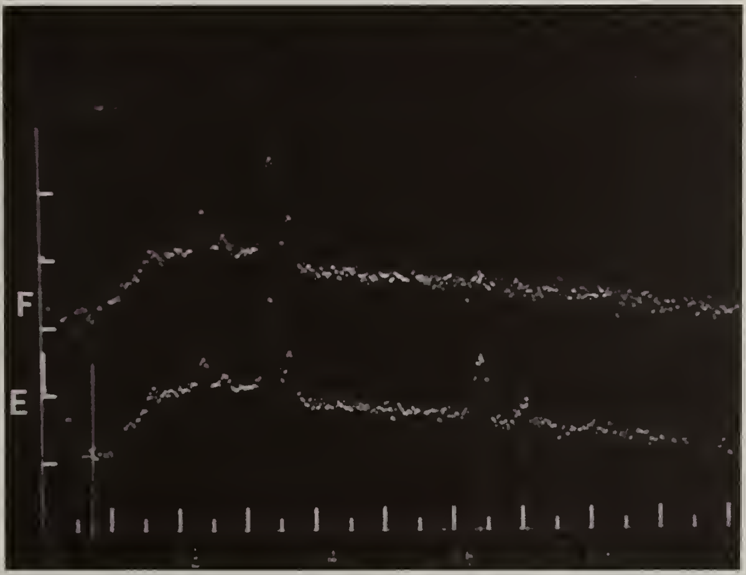

Fig. 7c. EDX spectra of regions E and F of Fig. 7 showing Fe penetration in the salt.

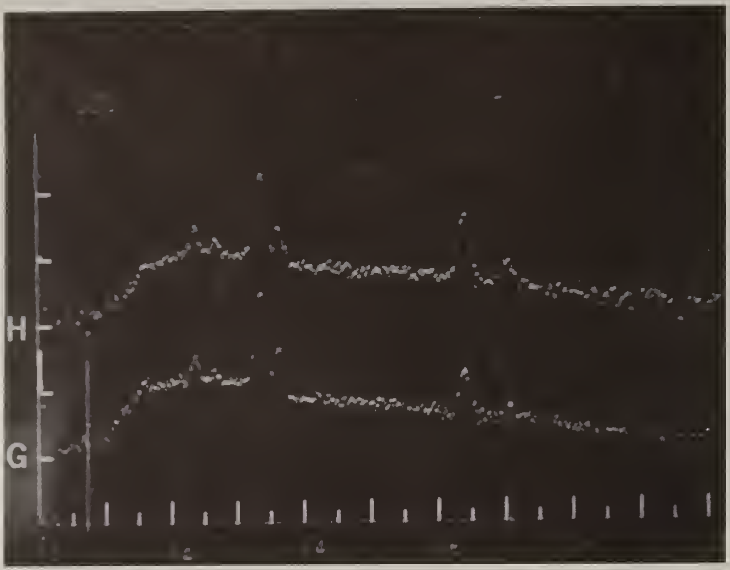

Fig. 7d. EDX spectra of regions G and H of Fig. 7 showing Fe penetration in the salt.

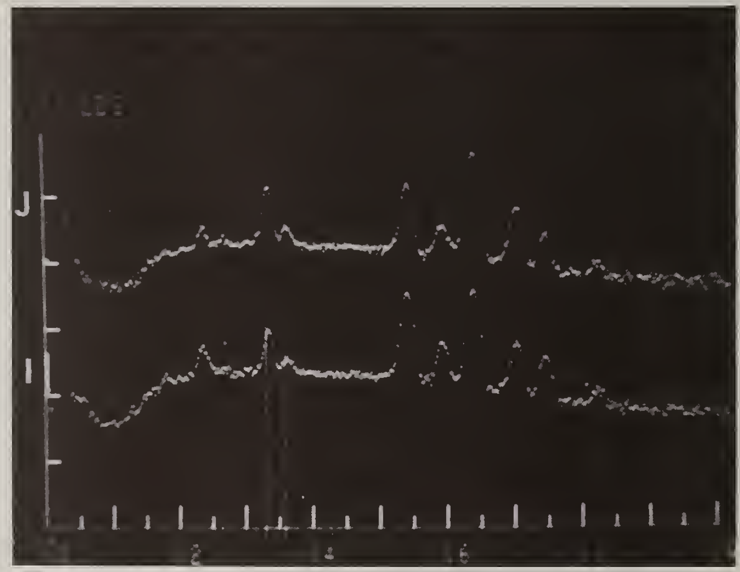

Fig. 7e. EDX spectra of regions I and J of Fig. 7 showing areas of high Cr and low Ni concentration.

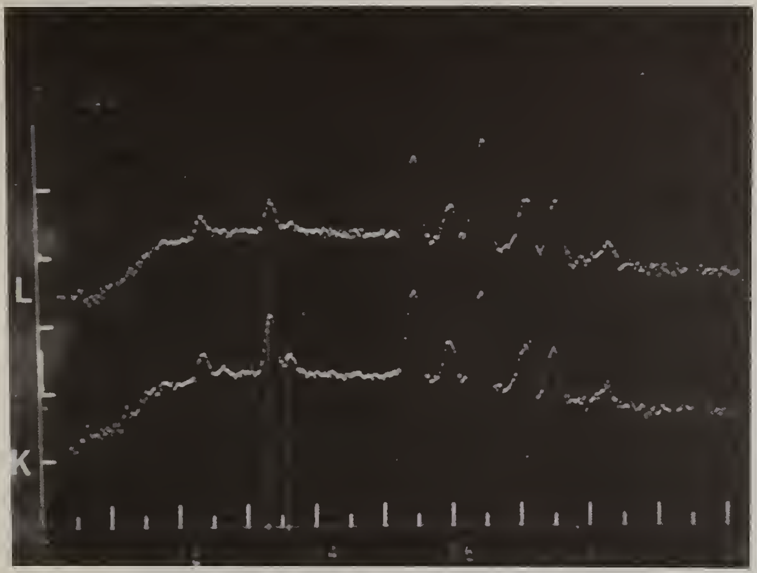

Fig. 7f. EDX spectra of regions K and L of Fig. 7 showing areas of high Cr concentration formed on stainless steel edge.

Fig. 8. SEM micrograph, 2000 X, of stainless steel-salt deposit reaction zone. Lettered regions correspond to labeled EDX spectra, Figs. 8a-8j. Specimen temperature 590°C; gas stream oxygen rich.

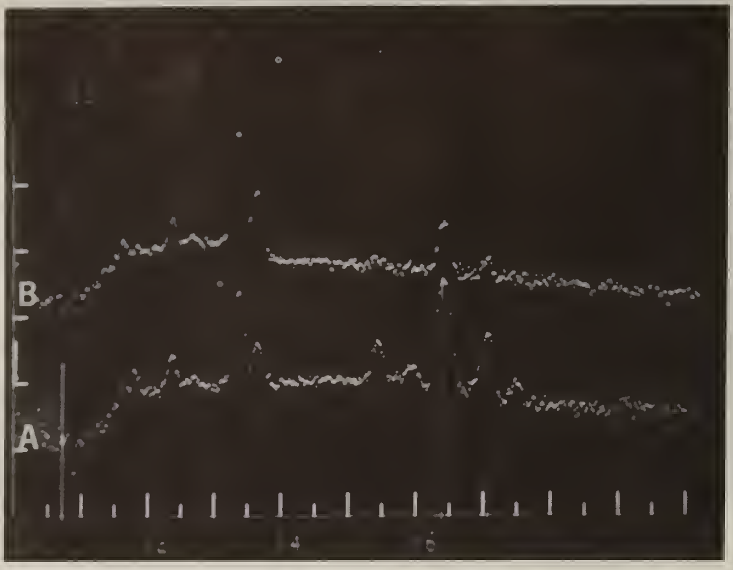

Fig. 8a. EDX spectra of regions A and B of Fig. 8 showing Fe penetration in the salt deposit.

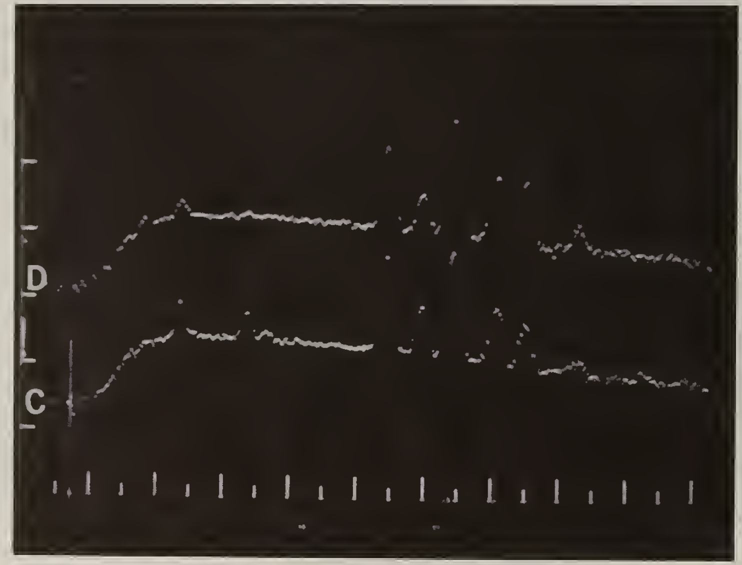

Fig. 8b. EDX spectra of regions C and D of Fig. 8 showing area of high Cr concentration as compared to bulk stainless.

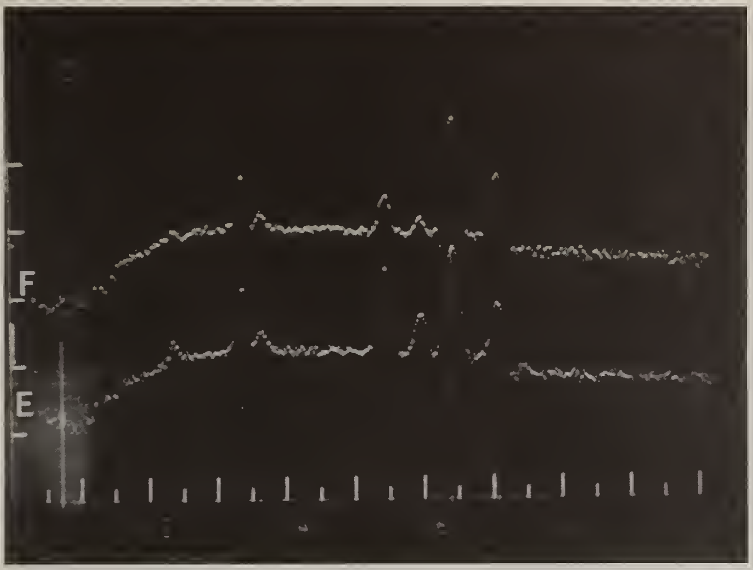

Fig. 8c. EDX spectra of regions E and F of Fig. 8 showing area of high Cr and high Fe concentration with absence of Ni at the stainless steel-salt interface.

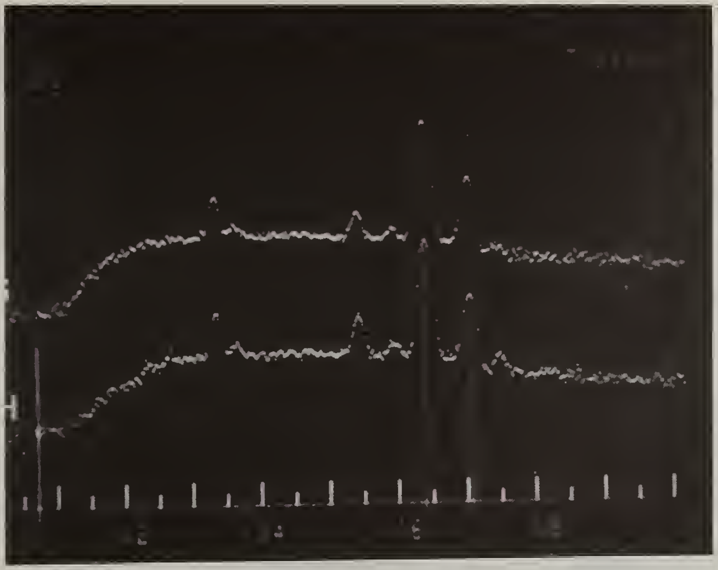

Fig. 8d. EDX spectra of regions G and H of Fig. 8 showing area of high Fe and low Cr concentration with traces of Ni at the stainless steel-salt interface.

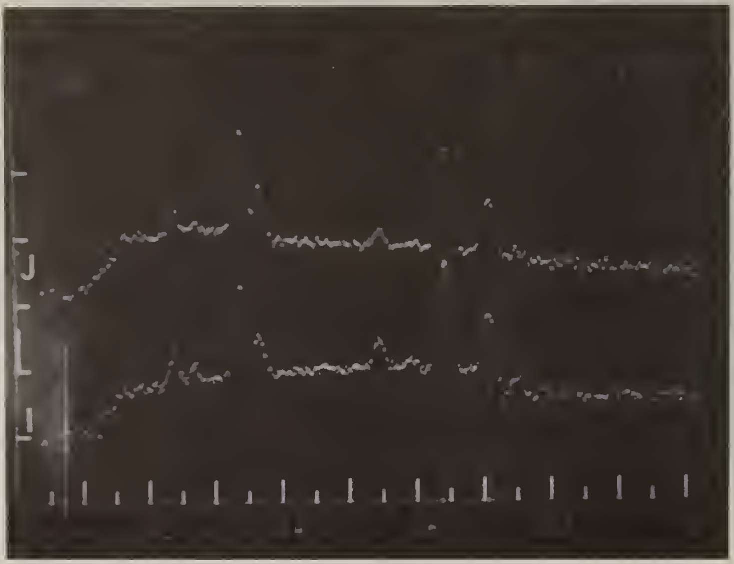

Fig. 8e. EDX spectra of regions I and J of Fig. 8 showing penetration of Fe and Cr in the salt deposit.

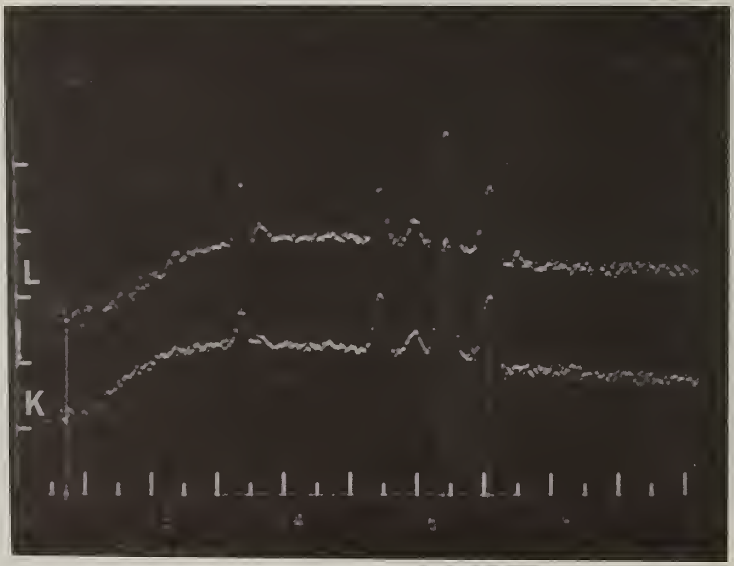

Fig. 8f. EDX spectra of regions K and L of Fig. 8 showing area of high Fe and low Cr concentration with absence of Ni at the stainless-steel salt interface.

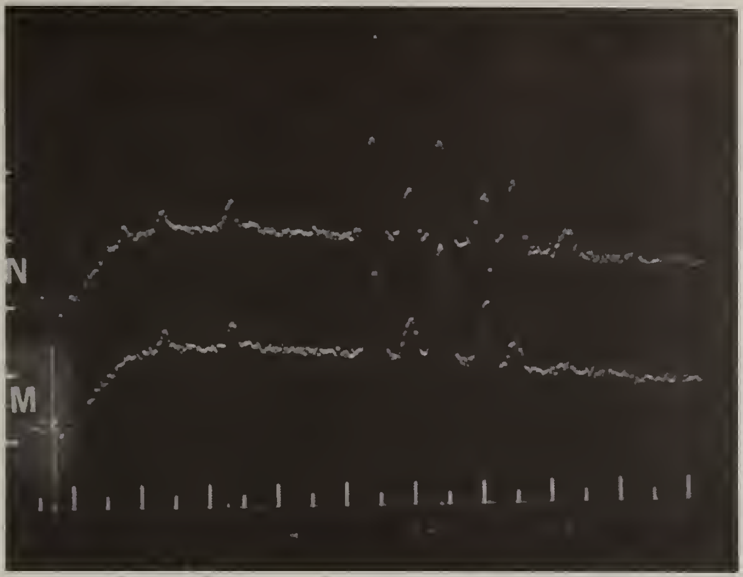

Fig. 8g. EDX spectra of regions M and N of Fig. 8 showing areas of high Cr and high Ni concentration as compared to low Cr and low Ni below the stainless steel-salt deposit interface but within the reaction band.

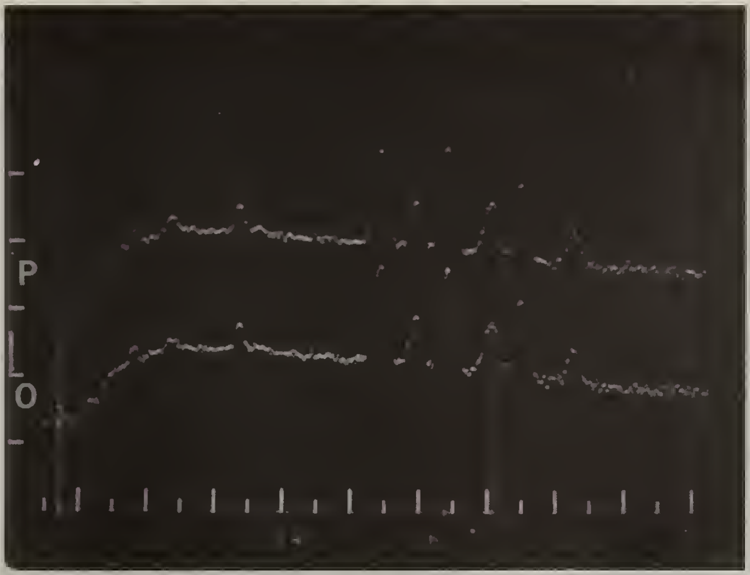

Fig. 8h. EDX spectra of regions O and P of Fig. 8 showing areas of high Cr and high Ni concentration below the stainless steel-salt deposit interface, but within the reaction band.

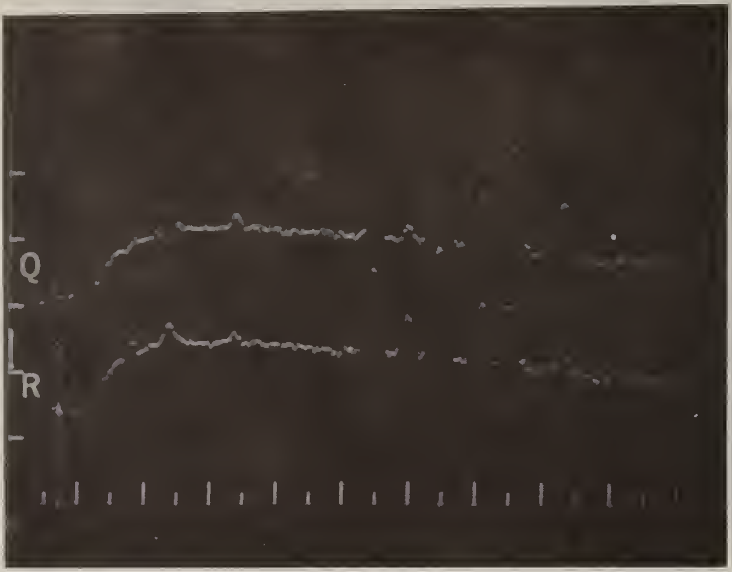

Fig. 8i. EDX spectra of regions Q and R of Fig. 8 indicating a region of very high Ni concentration in a matrix of high Cr concentration as compared to the bulk stainless steel.

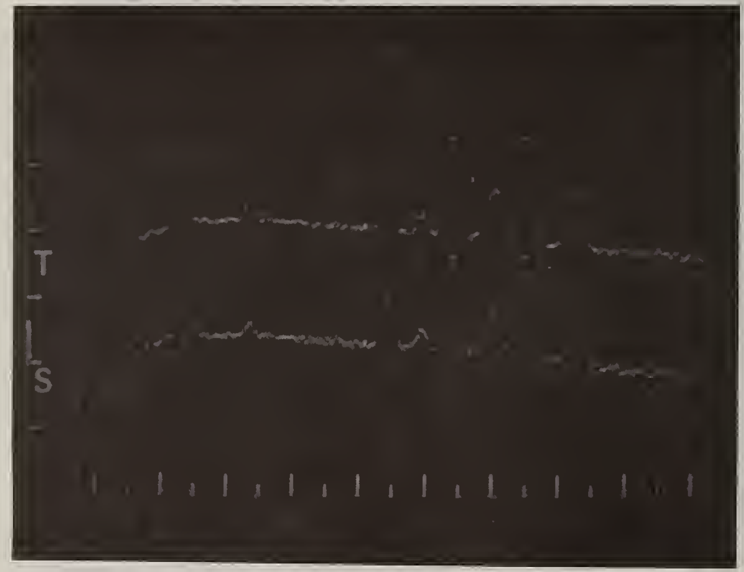

Fig. 8j. EDX spectra of regions S and T of Fig. 8 showing high Ni concentration with the high Cr concentration matrix.

Fig. 9. SEM micrograph, 2000 X, of stainless steel-salt deposit reaction zone. Lettered regions correspond to labeled EDX spectra Figs. 9a-9e. Specimen temperature 400°C; gas stream oxygen rich.

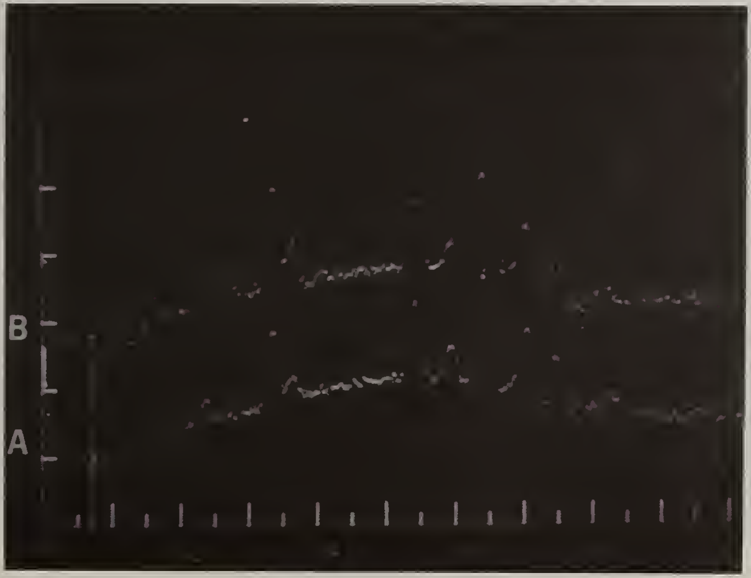

Fig. 9a. EDX spectra of regions A and B of Fig. 9 showing areas of low Ni concentration on the stainless steel interface.

Fig. 9b. EDX spectra of regions C and D of Fig. 9 showing areas of low Ni concentration on the stainless steel interface.

Fig. 9c. EDX spectra of regions E and F of Fig. 9 indicating Fe penetration into the salt deposit.

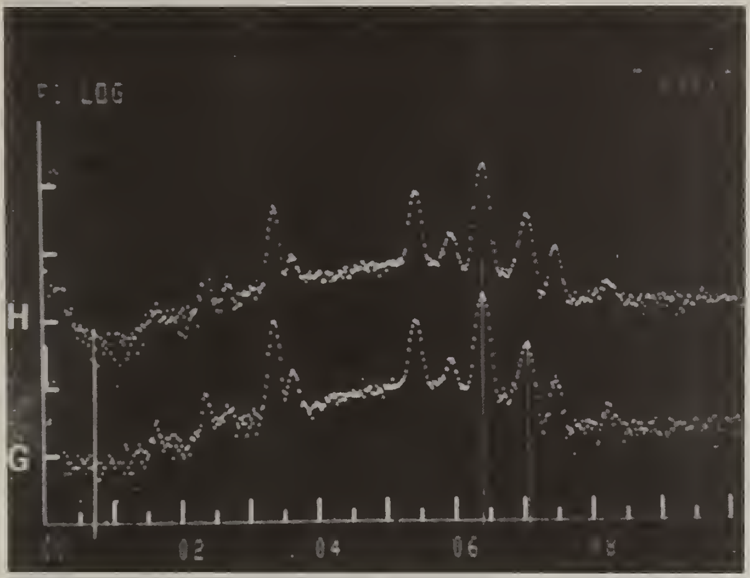

Fig. 9d. EDX spectra of regions G and H of Fig. 9 showing areas of low Ni concentration on the stainless steel interface.

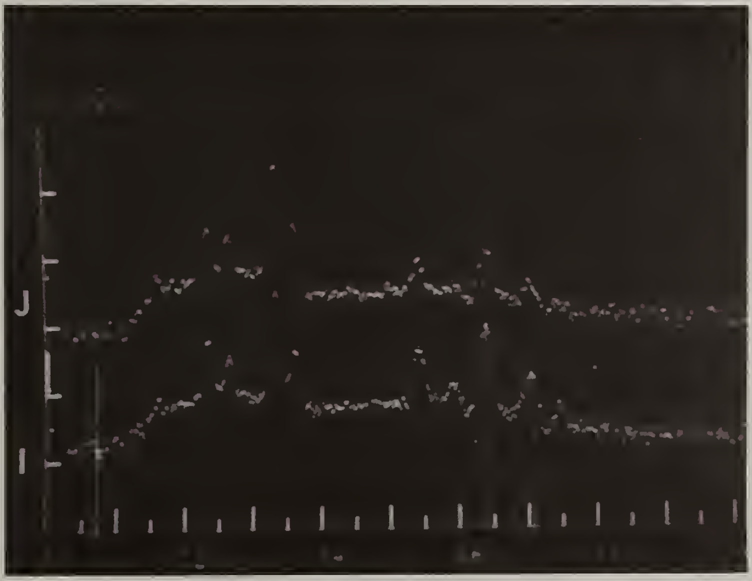

Fig. 9e. EDX spectra of regions I and J of Fig. 9 indicating Fe and Cr penetration into the salt deposit.

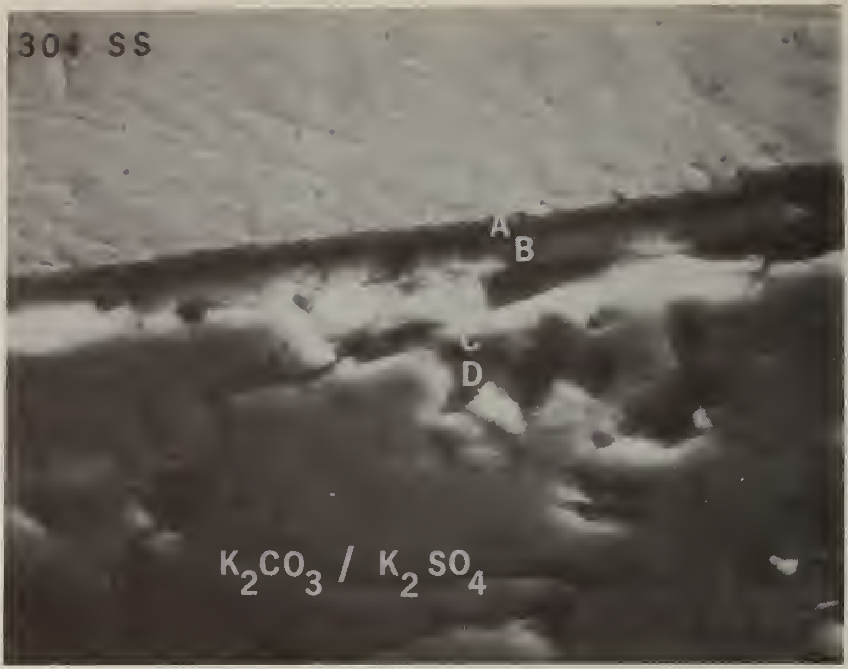

Fig. 10. SEM micrograph, 2000 X, of stainless steel-salt deposit reaction zone. Lettered regions correspond to labeled EDX spectra Figs. 10a and 10b. Specimen temperature 400°C; gas stream oxygen rich.

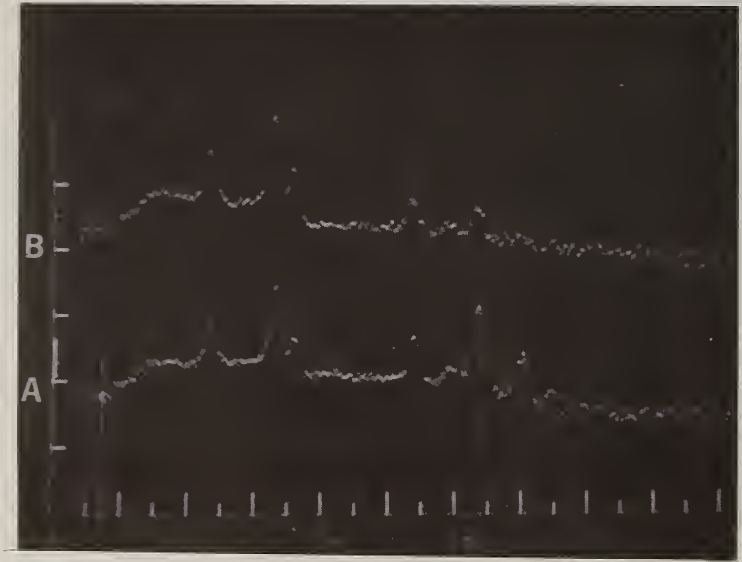

Fig. 10a. EDX spectra of regions A and B of Fig. 10 showing areas of Fe and Cr penetration into an area of potassium and sulfur.

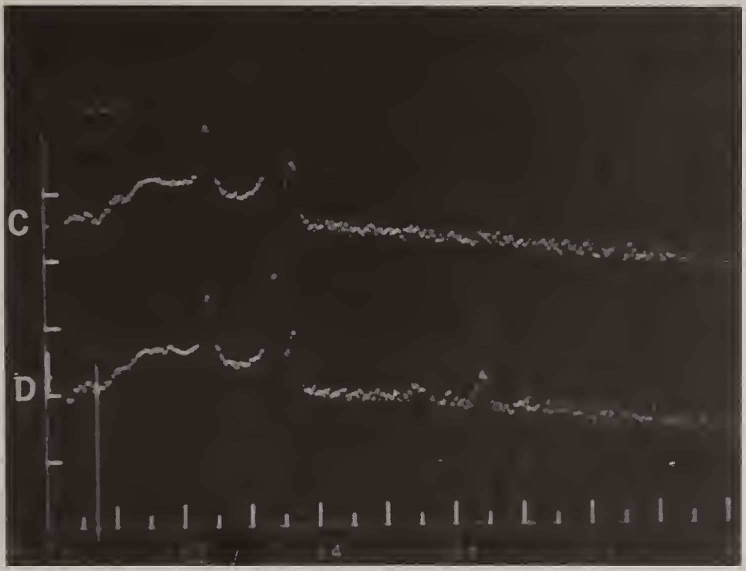

Fig. 10b. EDX spectra of regions C and D of Fig. 10 showing farther penetration of Fe and Cr into the salt deposit region.

Fig. 11. Section of Type 304 stainless steel tubing after exposure to K_2CO_3/K_2SO_4 seeded fuel rich hot gas stream. Note formation of 0.8 mm deposit on upper surface. Tube temperature 400°C. 6 X.

Fig. 12. Section of Type 304 stainless steel tubing after exposure to K_2CO_3/K_2SO_4 seeded fuel rich hot gas stream. Tube temperature 500°C. 6 X.

Fig. 13. Section of Type 304 stainless steel tubing after exposure to K_2CO_3/K_2SO_4 seeded fuel rich hot gas stream. Note formation of thin deposit on upper surface. Tube temperature 590°C. 6 X.

Fig. 14. SEM micrograph, 2000 X, of stainless steel-salt deposit reaction zone. Lettered regions correspond to labeled EDX spectra, Figs. 14a to 14f. Specimen temperature 500°C; gas stream fuel rich.

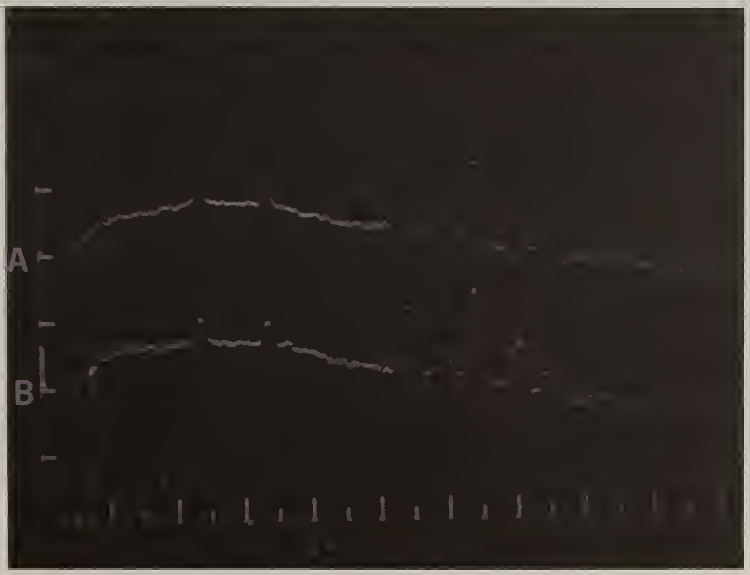

Fig. 14a. EDX spectra of regions A and B of Fig. 14 pointing out areas of high Cr concentration and low Ni concentration on the stainless steel interface.

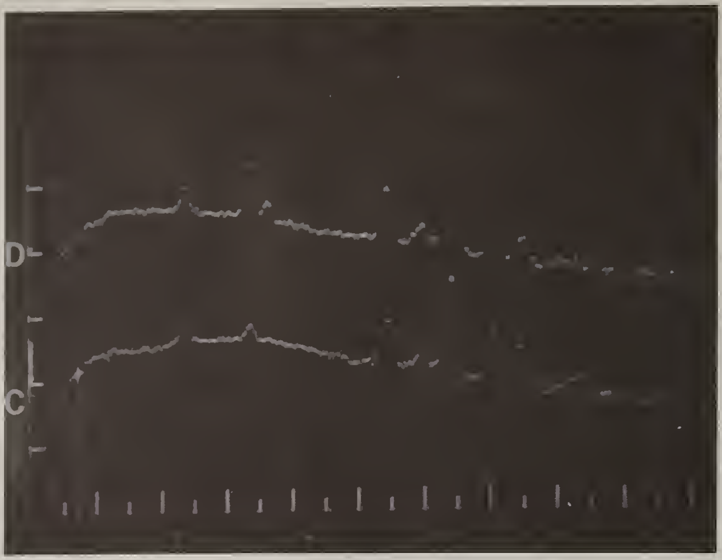

Fig. 14b. EDX spectra of regions C and D of Fig. 14 indicating areas of low Cr and low Ni concentration at the stainless steel interface.

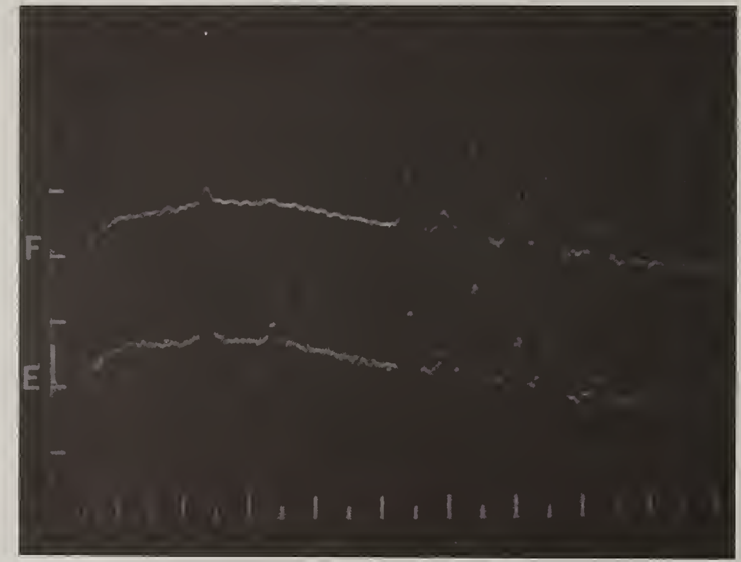

Fig. 14c. EDX spectra of regions E and F of Fig. 14 showing areas of high Ni and low Cr concentration at the stainless steel interface.

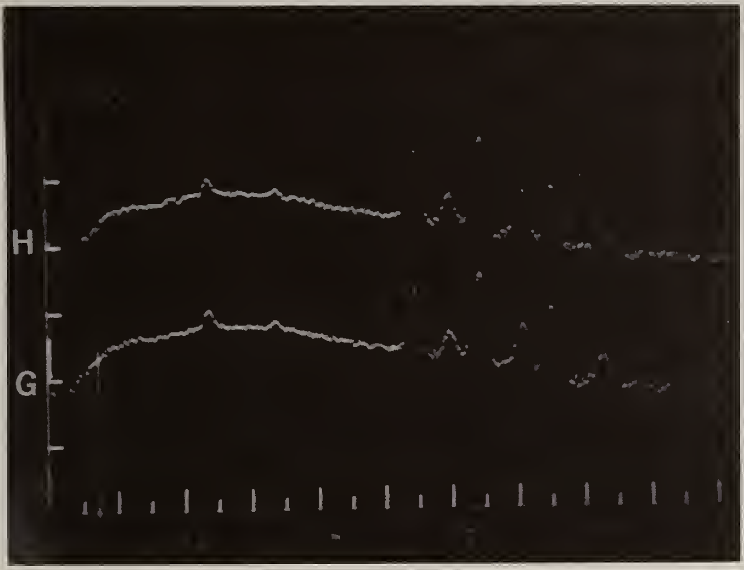

Fig. 14d. EDX spectra of regions G and H of Fig. 14 showing areas adjacent to E and F of high Ni concentration and low Cr concentration.

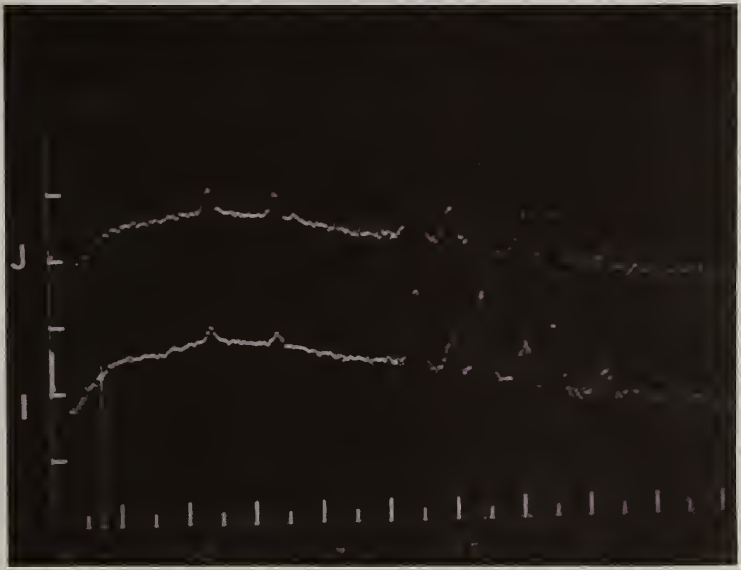

Fig. 14e. EDX spectra of regions I and J of Fig. 14 showing areas of high Ni and high Cr concentration at the interface.

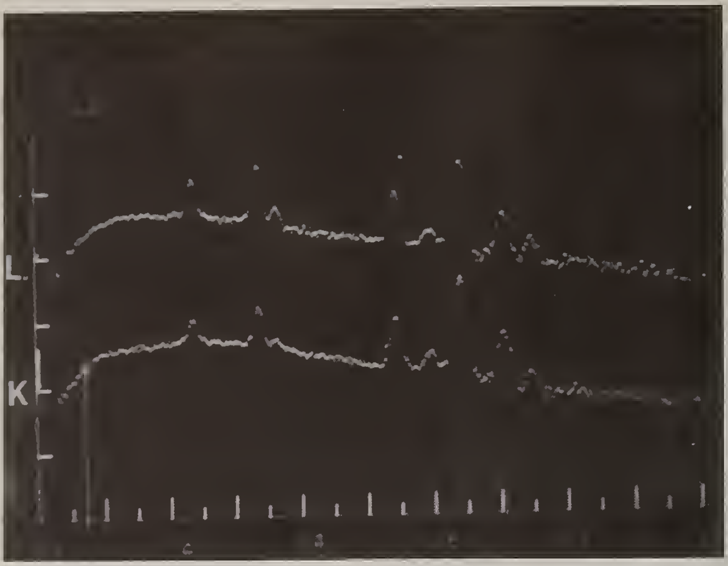

Fig. 14f. EDX spectra of regions K and L of Fig. 14 of areas below I and J showing low Cr and low Ni concentration.

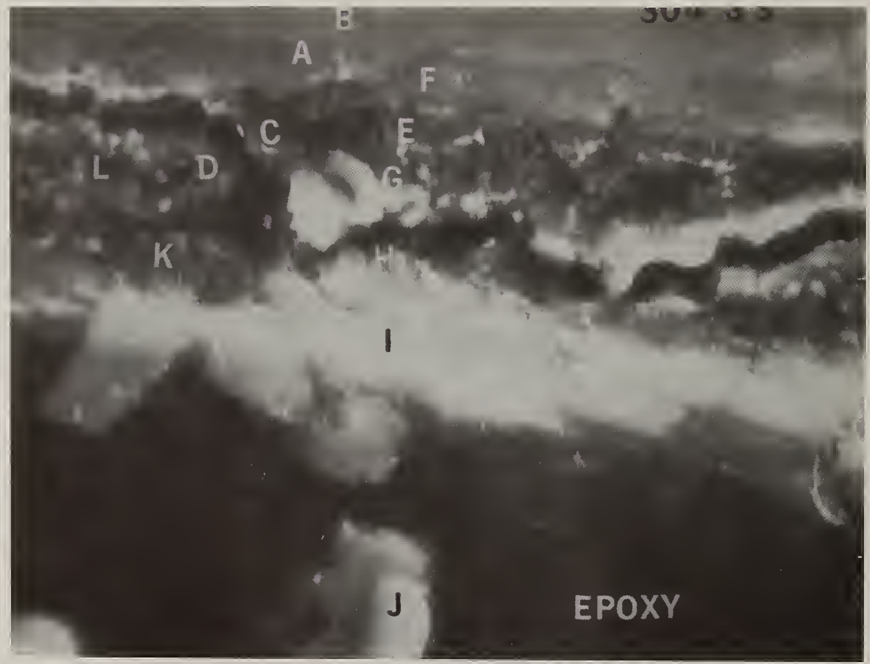

Fig. 15. SEM micrograph 2000 X, of stainless steel-salt deposit reaction zone. Lettered regions correspond to labeled EDX spectra, Figs. 15a to 15f. Specimen temperature 590°C gas stream fuel rich.

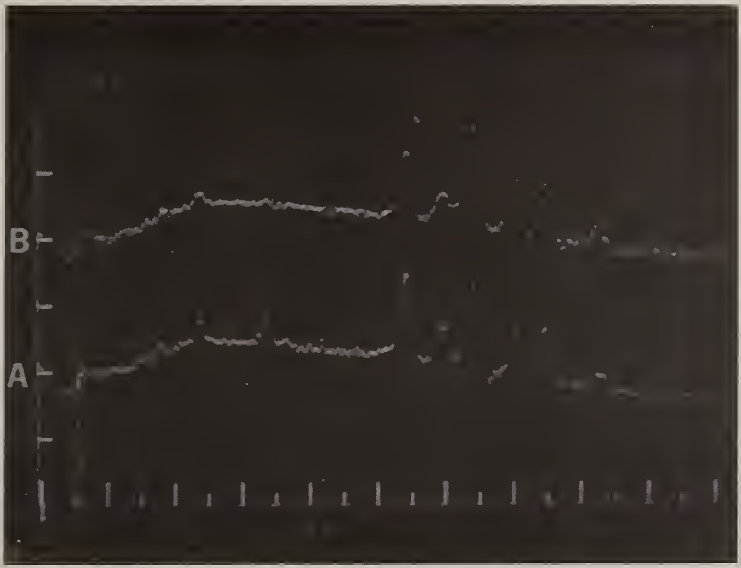

Fig. 15a. EDX spectra of regions A and B of Fig. 15 showing area of high Cr and high Ni concentration as compared to bulk stainless steel.

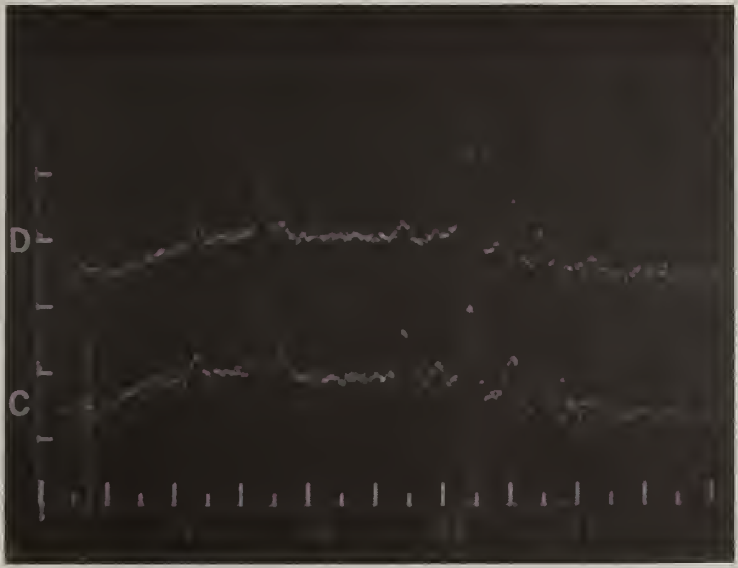

Fig. 15b. EDX spectra of regions C and D of Fig. 15 showing areas of high Fe, low Ni and low Cr concentration at the stainless steel-salt interface.

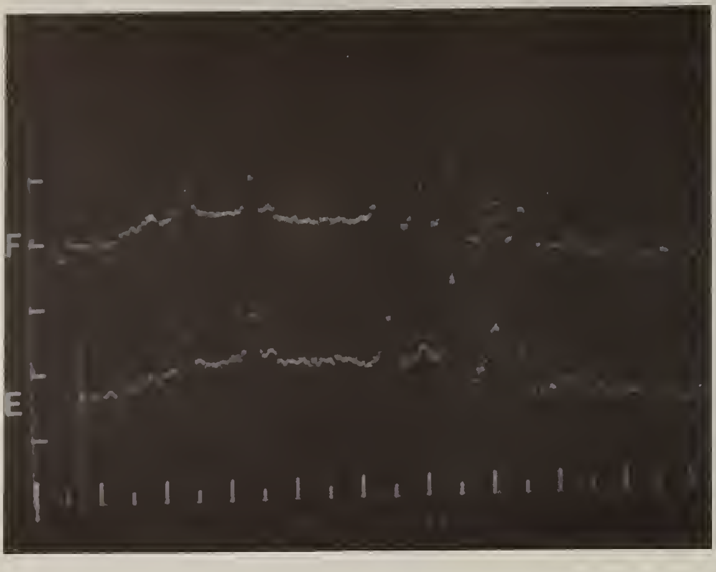

Fig. 15c. EDX spectra of region E of Fig. 15 indicating area of high Cr concentration with Ni and region F of Fig. 15 showing area of low Cr concentration with high Ni concentration.

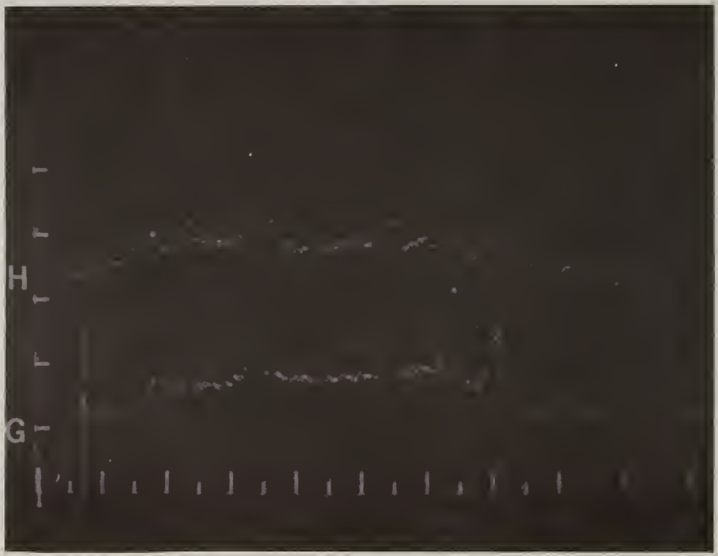

Fig. 15d. EDX spectra of regions G and H of Fig. 15 showing areas of high Fe and low Ni and low Cr concentrations at the stainless steel-deposit interface.

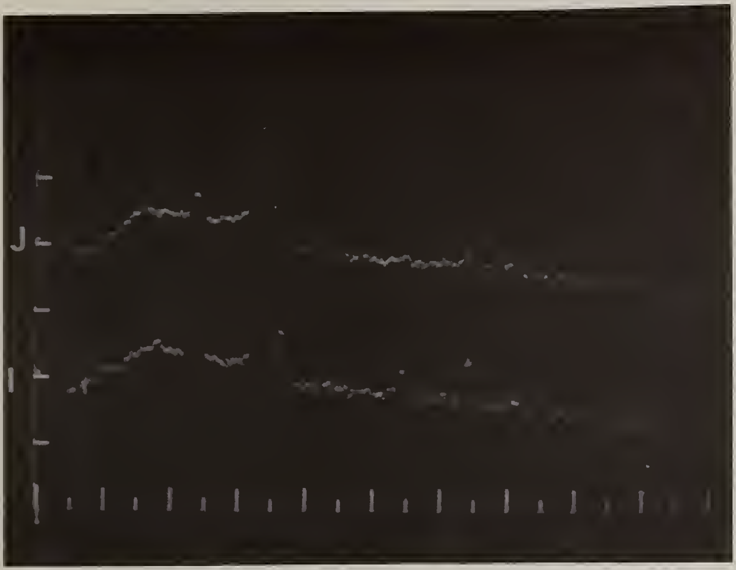

Fig. 15e. EDX spectra of regionsI and J of Fig. 15 showing Fe and Cr penetration into the salt deposit.

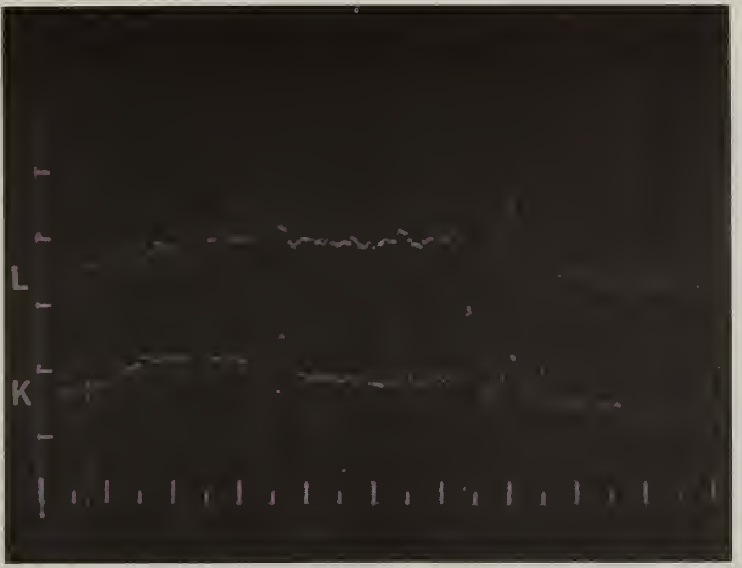

Fig. 15f. EDX spectra of regionsK and L of Fig. 15 showing areas of high Ni and low Cr concentration at the stainless steel-salt interface.

Fig. 16. Section of Type 304 stainless steel prior to exposure to the seeded hot gas stream. 6 X.

Fig. 17. SEM micrograph 4500 X, of section of Fig. 16 showing stainless steel edge.

Fig. 18. SEM micrograph (montage) 9000 X, of a section of Fig. 16 showing inclusions and pits in the stainless steel.